



OPEN ACCESS

EDITED BY

Nada Zamel,
Fraunhofer Institute for Solar Energy Systems
(ISE), Germany

REVIEWED BY

Zhiming Bao,
Tianjin University, China
Xiaohui Yan,
Shanghai Jiao Tong University, China
Yuze Hou,
Fraunhofer Institute for Solar Energy Systems
(ISE), Germany
Thomas Kadyk,
Helmholtz Association of German Research
Centres (HZ), Germany

*CORRESPONDENCE

Pablo A. García-Salaberri,
✉ pagsalab@ing.uc3m.es

RECEIVED 17 December 2023

ACCEPTED 18 March 2024

PUBLISHED 02 April 2024

CITATION

García-Salaberri PA, Das PK and Chaparro AM
(2024), Local oxygen transport resistance in
polymer electrolyte fuel cells: origin,
dependencies and mitigation.
Front. Energy Res. 12:1357325.
doi: 10.3389/fenrg.2024.1357325

COPYRIGHT

© 2024 García-Salaberri, Das and Chaparro.
This is an open-access article distributed under
the terms of the [Creative Commons Attribution
License \(CC BY\)](https://creativecommons.org/licenses/by/4.0/). The use, distribution or
reproduction in other forums is permitted,
provided the original author(s) and the
copyright owner(s) are credited and that the
original publication in this journal is cited, in
accordance with accepted academic practice.
No use, distribution or reproduction is
permitted which does not comply with these
terms.

Local oxygen transport resistance in polymer electrolyte fuel cells: origin, dependencies and mitigation

Pablo A. García-Salaberri^{1*}, Prodip K. Das² and Antonio M. Chaparro³

¹Departamento de Ingeniería Térmica y de Fluidos, Universidad Carlos III de Madrid, Leganés, Spain, ²School of Engineering, University of Edinburgh, Edinburgh, United Kingdom, ³Departamento de Energía, Centro de Investigaciones Energéticas, Medioambientales y Tecnológicas, Madrid, Spain

Next-generation polymer electrolyte fuel cells (PEFCs) require an integral design of the porous structure of electrodes at different scales to improve performance and enlarge durability while reducing cost. One of today's biggest challenges is the stable, high-performance operation at low Pt loading due to the detrimental effect of the local oxygen transport resistance caused by ionomer around catalyst sites. Hindered local oxygen transport arises from sluggish kinetics at the local reaction environment, that comprises adsorption at (wet) ionomer and Pt interfaces, and diffusivity of gas species in ionomer and water. Diverse factors affect oxygen transport, including operating conditions (relative humidity, temperature, and pressure), ionomer content and morphology, ionomer heterogeneity, porosity of carbon support, catalyst dispersity, and flooding. To attain performance and durability targets, it is essential to maximize the oxygen utilization of the catalyst layer by implementing enhanced membrane electrode assembly architectures. This involves employing advanced catalyst layer preparation techniques, including electrospraying, to generate optimized highly porous morphologies. Furthermore, achieving these targets necessitates the development of new materials with tailored properties, such as high permeability and porous ionomers, among other innovative strategies.

KEYWORDS

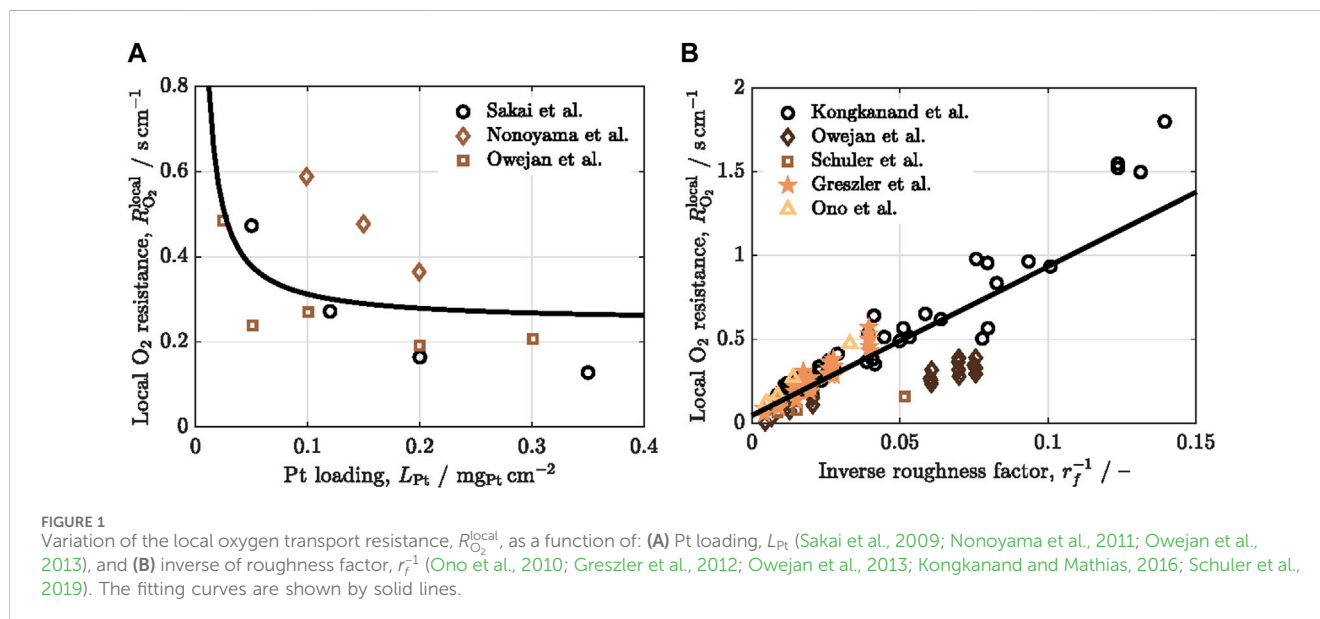
MEA, catalyst layer, oxygen resistance, performance, Pt loading, PEFC

1 Introduction

Polymer electrolyte fuel cells (PEFCs) stand at the forefront of sustainable energy technologies, holding the promise to revolutionize the landscape of power generation and transportation. As we navigate an era marked by the urgent need for cleaner and more efficient energy sources, PEFCs emerge as a beacon of innovation, offering a pathway toward reduced greenhouse gas emissions and enhanced energy security through the use of clean hydrogen as fuel (Fan et al., 2021; Yue et al., 2021). The appeal of PEFCs extends beyond their high energy conversion efficiency. Their scalability, rapid start-up times, and low operating temperatures make them well-suited for diverse applications, ranging from portable electronic devices to stationary power generation and fuel cell vehicles (Wee, 2007). Although the first demonstration of a fuel-cell passenger car dates back several decades, only two car manufacturers (Toyota and Hyundai) are actively producing fuel-cell cars at present

TABLE 1 Key target metrics for performance, cost, and durability of PEFC system for 2030 (interim) and 2050 (ultimate) (Das et al., 2023).

	Cost (US\$/kW)		Peak Efficiency (%)		System Lifetime (h)		Durability (thousand miles)	
	Interim target	Ultimate target	Interim target	Ultimate target	Interim target	Ultimate target	Interim target	Ultimate target
Car	40	30	65	70	5,000	8,000	150	150
Bus	40	30	65	70	25,000	30,000	500	500
Truck	80	60	68	72	25,000	30,000	1,000	1,200



(Das et al., 2023). Their market reach is constrained by various factors. One significant obstacle is the inadequate availability of hydrogen infrastructure and renewable hydrogen. However, perhaps the most pivotal impediment is the performance, durability, and cost of fuel-cell vehicles. Currently, these factors do not match up competitively with internal combustion engine (ICE) vehicles (Pollet et al., 2019; Whiston et al., 2019). To attain a more substantial market share and facilitate widespread commercialization of fuel cell vehicles (FCVs), there is a pressing need for enhancements that bring their performance, durability, and cost more in line with conventional ICE vehicles.

The primary performance, cost, and durability metrics for the PEFC system are detailed in Table 1, projecting values for both 2030 and 2050 as interim and ultimate targets, respectively. The data in Table 1 are a durability-adjusted cost of an 80-kW_{net} PEFC system based on a projection to high volume manufacturing at 100,000 units/year (Das et al., 2023; U.S. Department of Energy, 2022; James et al., 2021). The data underscore notable advancements in both performance and durability over recent decades, with the current status closely approaching the 2030 targets set by the U.S. Department of Energy (Das et al., 2023; U.S. Department of Energy, 2022). Despite these positive strides, the present cost of PEFC systems for passenger cars remains above US\$50/kW, necessitating a further 40% reduction to meet the ultimate target of US\$30/kW (Cullen et al., 2021; James et al., 2021).

While the cost, performance, and durability of fuel cells are intricately linked, there is a noteworthy effort to decrease the cost of fuel cell materials of the membrane electrode assembly (MEA), with a specific focus on Pt catalysts, given their substantial contribution to overall fuel cell cost (Nonoyama et al., 2011; Kongkanand and Mathias, 2016; Ganesan and Narayanasamy, 2019; Jiao et al., 2021). Many researchers and FCV manufacturers have already provided avenues for reducing Pt loading in catalyst layers, including Nissan, Toyota, and General Motors. They also noted that there is a lack of understanding about the performance of low Pt-loaded electrodes, which stems from the concentration polarization at low Pt loading. As shown in Figure 1A, when the Pt loading decreases, the local oxygen transport resistance through the thin ionomer film covering the Pt particles increases significantly (Sakai et al., 2009; Ono et al., 2010; Nonoyama et al., 2011; Greszler et al., 2012; Owejan et al., 2013; Kongkanand and Mathias, 2016; Schuler et al., 2019). Consequently, the local oxygen transport resistance at low Pt loading has been attributed to the ionomer coating around the Pt surface. Efficient proton conduction at low Pt loading can be achieved by adjusting the ionomer-to-carbon weight ratio in the catalyst layer (Sabarirajan et al., 2020). However, achieving optimal oxygen transport simultaneously is complicated.

The efficient transport of oxygen to the catalyst sites is crucial for minimizing activation and concentration polarizations as well as ensuring the availability of oxygen for the electrochemical reaction

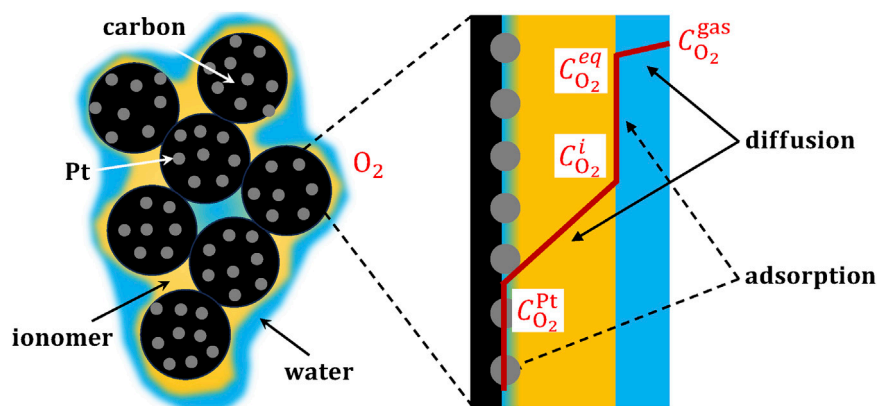


FIGURE 2

Schematic of the local oxygen transport resistance, composed of adsorption at (wet) ionomer and Pt interfaces, and diffusion across water and ionomer thin films.

during the reduction of oxygen molecules at the cathode catalyst layer. As shown in Figure 2, oxygen transport within the catalyst layer is intricately connected to both the adsorption of oxygen from the gas phase onto the catalyst surface through the ionomer and the subsequent diffusion of oxygen within the ionomer (Nonoyama et al., 2011). Experimental measurement of oxygen transport resistance in the catalyst layer involves distinguishing between molecular/Knudsen diffusion and local resistance through the thin ionomer films to the catalyst surface (Nonoyama et al., 2011; Weber et al., 2012; Wang et al., 2017). Researchers have utilized various methods to assess oxygen transport resistance in the catalyst layer, among which are the gas crossover method (Iden et al., 2013a) and the limiting current method (Baker et al., 2009; Nonoyama et al., 2011; Greszler et al., 2012).

Greszler et al. (Greszler et al., 2012) emphasized that the partial pressure of oxygen at the Pt surface can experience a notable reduction at low Pt loading. This reduction can result in severe performance degradation of fuel cells, particularly during high-power operations. It was concluded that oxygen transport resistance is inversely proportional to Pt loading or Pt surface area. Nonoyama et al. (Nonoyama et al., 2011) experimentally measured oxygen transport resistance using limiting current density. They identified three components of oxygen transport resistance: molecular diffusion, Knudsen diffusion, and permeation through the ionomer film. Their findings indicated that the primary contributor to the transport resistance is the permeation through the ionomer film. Wang et al. (Wang et al., 2017) similarly concluded that local transport significantly influences the oxygen transport resistance to active catalyst sites. They found that it could account for up to 77% of the total cathode catalyst layer resistance when Pt loading is reduced to $0.05 \text{ mg}_{\text{Pt}} \text{ cm}^{-2}$. Although previous studies associated performance loss with low Pt loading due to local transport resistance, Owejan and colleagues delved deeper into the matter (Owejan et al., 2013). They emphasized that transport resistance through the ionomer coating is not solely a function of Pt loading but is also influenced by both Pt surface area and particle dispersion. Indeed, as shown in Figure 1B, the local oxygen transport resistance depends linearly on the roughness factor, defined as the product of the Pt loading and the electrochemical surface area (ECSA). Moreover, factors such as

oxygen mole fraction, relative humidity, operating pressure, and temperature have been identified as influencing local transport resistance (Choo et al., 2015; Shen et al., 2017). Researchers have proposed that the local oxygen transport resistance may not solely arise from oxygen transport within the thin ionomer film. Instead, it might be an apparent interfacial resistance resulting from the interaction between the acid site of the ionomer and the polarized catalyst (Liu et al., 2015).

Certainly, the intricate dynamics of oxygen transport resistance, involving factors such as electrode thickness, Pt loading, Pt surface area, and particle dispersion, pose a substantial challenge that can hinder the overall performance of fuel cells. Consequently, it is crucial to delve into the specifics of local oxygen transport resistance, emphasizing its origin, dependencies, and potential strategies for mitigation. Understanding these intricacies is paramount for enhancing and optimizing fuel cell performance and reducing cost. Indirect strategies to improve oxygen transport, such as flow-field design, are not addressed here.

2 Dependencies

The most influential factors on the local oxygen transport resistance are discussed below, including: i) relative humidity, temperature and pressure, ii) ionomer content and morphology, iii) ionomer distribution, iv) carbon porosity, and v) additional factors. The factors organized in order of their impact on the local oxygen transport resistance are listed in Table 2. The most influential factors appear to be those related to the amount and permeability of ionomer surrounding catalyst particles and the number of electrochemically activated sites (i.e., ionomer porosity, I/C ratio, and relative humidity).

2.1 Effect of relative humidity, temperature and pressure

The oxygen flux from the bulk gas space toward the catalyst surface can be decomposed into three mechanisms (see

TABLE 2 Impact of factors that affect the local oxygen transport resistance, according to the relative variation of the resistance value. The impact is categorized as low, medium, medium-high and high.

Factor	Action	Relative variation	Impact	References
Ionomer porosity	Incorporating mesopores of 5–10 nm in diameter	0.37 to 0.08 s cm ⁻¹	High	Cheng et al. (2022b)
		-78.3%		
I/C ratio	Decreasing I/C from 1 to 0.2	0.77 to 0.14 s cm ⁻¹	High	Wang et al. (2019), Sun et al. (2021), Yakovlev et al. (2021)
		-77.9%		
Relative humidity	Increasing RH from 0.2 to 0.9	0.27 to 0.09 s cm ⁻¹	High	Kudo et al. (2016), Conde et al. (2019), Cetinbas et al. (2020), Poojary et al. (2020)
		-66.7%		
Temperature	Increasing <i>T</i> from 40 C to 80 C	0.49 to 0.23 s cm ⁻¹	Medium-High	(Shen et al., 2017; Conde et al., 2019; Yakovlev et al., 2021)
		-53.1%		
Ionomer permeability	Increasing <i>P</i> _{O₂} from 20 barrer to 85 barrer	0.28 to 0.18 s cm ⁻¹	Medium-High	Macauley et al. (2022)
		-35.7%		
		0.21 to 0.09 s cm ⁻¹		
		-57.1%		
Carbon support accessibility	Optimizing mesoporous fraction between 4–7 nm	0.17 to 0.09 s cm ⁻¹	Medium-High	Yarlagadda et al. (2018)
		-47.06%		
Carbon support porosity	Removing nanopores in carbon support (e.g., Vulcan)	0.42 to 0.26 s cm ⁻¹	Medium-High	Ramaswamy et al. (2020), Yarlagadda et al. (2022)
		-38.1%		
Ionomer <i>EW</i>	Increasing <i>EW</i> from 720 to 1,100 g mol ⁻¹	0.06–0.13 s cm ⁻¹	Medium-High	Ramaswamy et al. (2021)
		116.7%		
	Increasing <i>EW</i> from 825 to 1,100 g mol ⁻¹	0.27 to 0.17 s cm ⁻¹	Medium-High	Poojary et al. (2020)
		-37.0%		
Ionomer uniformity	Carbon support functionalization	0.7 to 0.5 s cm ⁻¹	Medium	Orfanidi et al. (2017)
		-28.6%		
Pressure	Decreasing <i>p</i> from 1.5 bar to 1.2 bar	0.36–0.39 s cm ⁻¹	Low	Shen et al. (2017)
		7.7%		

Figure 2): i) oxygen adsorption from the gas phase into the ionomer, ii) oxygen diffusion inside the ionomer, and iii) oxygen adsorption from the ionomer to the catalyst surface (Nonoyama et al., 2011). In a first approximation, the contribution of water films present at either the inner and/or outer surfaces of the ionomer film is neglected due to their lower effect on the local oxygen transport resistance compared to the above three mechanisms. The expressions of the oxygen flux, *N*^{*i*}_{O₂}, for each process are given by

$$N_{O_2}^i = k_{g/i}(C_{O_2}^{eq} - C_{O_2}^i) \tag{1.1}$$

$$N_{O_2}^i = D_{O_2,i}^{eff} \frac{(C_{O_2}^i - C_{O_2}^{Pt})}{\delta_i} \tag{1.2}$$

$$N_{O_2}^i = k_{i/Pt} C_{O_2}^{Pt} \tag{1.3}$$

where *C*_{O₂}^{eq}, *C*_{O₂}^{*i*} and *C*_{O₂}^{Pt} are the equilibrium oxygen concentration, oxygen concentration at the ionomer interface (adjacent to the gas side), and the oxygen concentration at the catalyst surface,

respectively, *k*_{*g*/*i*} and *k*_{*i*/*Pt*} are the rate constants for oxygen adsorption at the gas/ionomer and ionomer/Pt interfaces, *D*_{O₂,*i*}^{eff} is the effective diffusivity of oxygen in ionomer, and *δ*_{*i*} is the ionomer film thickness.

The equilibrium oxygen concentration, *C*_{O₂}^{eq}, can be expressed in terms of the solubility coefficient, *S*_{O₂}^{*g*/*i*}, as (Shen et al., 2017)

$$C_{O_2}^{eq} = S_{O_2}^{g/i} RT C_{O_2}^{gas} \tag{2}$$

where *R* is the universal gas constant and *T* is the temperature.

Considering that the above three transport processes are arranged in series, the overall oxygen transport resistance is

$$R_{O_2}^i = \frac{C_{O_2}^{gas}}{N_{O_2}^i} = \left[\frac{\delta_i}{D_{O_2,i}^{eff}} + \frac{1}{k_{g/i}} + \frac{1}{k_{i/Pt}} \right] \frac{1}{RT} \frac{1}{S_{O_2}^{g/i}} \tag{3}$$

which can be re-expressed in terms of the oxygen equilibrium concentration, *C*_{O₂}^{eq}, and the oxygen concentration in the bulk gas space, *C*_{O₂}^{gas}, through Eq. 2

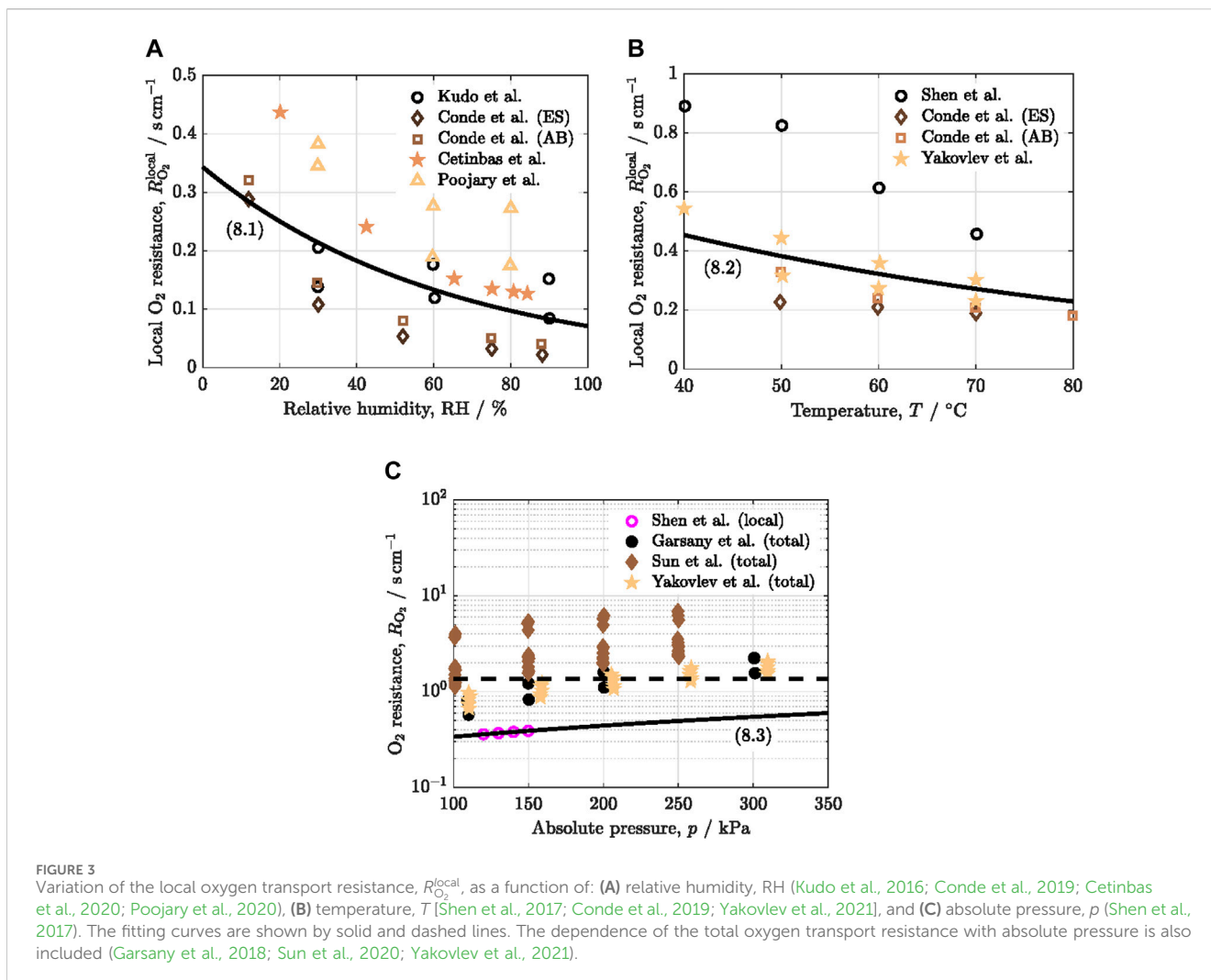


FIGURE 3 Variation of the local oxygen transport resistance, $R_{O_2}^{\text{local}}$, as a function of: (A) relative humidity, RH (Kudo et al., 2016; Conde et al., 2019; Cetinbas et al., 2020; Poojary et al., 2020), (B) temperature, T (Shen et al., 2017; Conde et al., 2019; Yakovlev et al., 2021), and (C) absolute pressure, p (Shen et al., 2017). The fitting curves are shown by solid and dashed lines. The dependence of the total oxygen transport resistance with absolute pressure is also included (Garsany et al., 2018; Sun et al., 2020; Yakovlev et al., 2021).

$$R_{O_2}^i = \left[\frac{\delta_i}{D_{O_2,i}^{\text{eff}}} + \frac{1}{k_{g/i}} + \frac{1}{k_{i/Pt}} \right] \frac{C_{O_2}^{\text{gas}}}{C_{O_2}^{\text{eq}}} \quad (4)$$

The relationship between the equilibrium and bulk oxygen concentrations is given by the adsorption isotherm at the gas/ionomer interface. Considering a Langmuir-type isotherm, $C_{O_2}^{\text{eq}} \approx K_L C_{O_2}^{\text{gas}} / (1 + K_L C_{O_2}^{\text{gas}})$, as suggested by Shen et al. (Shen et al., 2017), we yield

$$R_{O_2}^i = \left[\frac{\delta_i}{D_{O_2,i}^{\text{eff}}} + \frac{1}{k_{g/i}} + \frac{1}{k_{i/Pt}} \right] \frac{1 + K_L C_{O_2}^{\text{gas}}}{K_L} \quad (5)$$

where K_L is the Langmuir rate constant.

The local oxygen resistance per unit of active catalyst surface area, $R_{O_2}^i$, and the local oxygen resistance per unit of geometric area, $R_{O_2}^{\text{local}}$, are related by the roughness factor (Sánchez-Ramos et al., 2021; Sánchez-Ramos et al., 2022)

$$R_{O_2}^i = r_f R_{O_2}^{\text{local}}; r_f = L_{Pt} a_{\text{ecsa}} \quad (6)$$

where L_{Pt} is the Pt loading and a_{ecsa} is the ECSA.

Introducing the above relationship, $R_{O_2}^{\text{local}}$ turns out to be

$$R_{O_2}^{\text{local}} = \left[\frac{\delta_i}{D_{O_2,i}^{\text{eff}}} + \frac{1}{k_{g/i}} + \frac{1}{k_{i/Pt}} \right] \frac{1 + K_L C_{O_2}^{\text{gas}}}{K_L} \frac{1}{r_f} \quad (7)$$

which is inversely proportional to the roughness factor, as observed in previous experimental studies (see Figure 1B) (Greszler et al., 2012; Weber and Kusoglu, 2014).

The effect of the main operating conditions, relative humidity, temperature and pressure, on the local oxygen transport resistance reported by various authors is shown in Figure 3 (Kudo et al., 2016; Shen et al., 2017; Garsany et al., 2018; Conde et al., 2019; Cetinbas et al., 2020; Poojary et al., 2020; Sun et al., 2020; Yakovlev et al., 2021; Cheng et al., 2022a). The fitting curves are added to the collected datasets. $R_{O_2}^{\text{local}}$ decreases with increasing relative humidity and temperature, while it increases with increasing pressure. The fitted correlations are equal to

$$R_{O_2}^{\text{local}} = 0.34 \exp(-1.58RH) \text{ s cm}^{-1} \quad (8.1)$$

$$R_{O_2}^{\text{local}} = 97 \exp(-0.017T) \text{ s cm}^{-1} \quad (8.2)$$

$$R_{O_2}^{\text{local}} = 1.37 + 4.66 \times 10^{-6} p \text{ s cm}^{-1} \quad (8.3)$$

where RH, T and p are expressed in SI units.

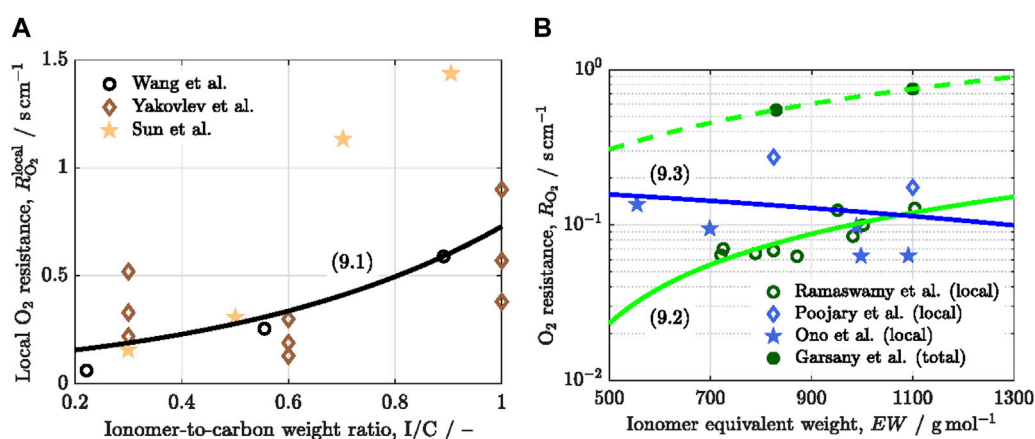


FIGURE 4
Variation of the local oxygen transport resistance, $R_{O_2}^{\text{local}}$, as a function of: (A) ionomer-to-carbon weight ratio, I/C (Wang et al., 2019; Sun et al., 2021; Yakovlev et al., 2021), and (B) ionomer equivalent weight, EW [Poojary et al., 2020; Ramaswamy et al., 2021; Ono et al., 2013,]. The fitting curves are shown by solid and dashed lines. The dependence of the total oxygen transport resistance with equivalent weight is also included (Garsany et al., 2018). Opposite trends are observed in the effect of equivalent weight.

The positive effect of relative humidity on reducing $R_{O_2}^{\text{local}}$ is ascribed to two main factors: i) increase of the effective diffusivity of oxygen in ionomer caused by a higher water content (Kudo et al., 2016; Shen et al., 2017; Poojary et al., 2020), and ii) increase of ECSA and therefore increase of the roughness factor (Cetinbas et al., 2020). The relative contribution of each factor varies between different literature sources. Kudo et al. (Kudo et al., 2016) found that the dominant factor was the increase of oxygen permeability originating from an increase of oxygen effective diffusivity, while the oxygen solubility remained almost constant with relative humidity. A similar explanation was provided by Shen et al. (Shen et al., 2017) and Poojary et al. (Poojary et al., 2020). In contrast, the numerical work of Cetinbas et al. (Cetinbas et al., 2020) ascribed entirely the reduction of $R_{O_2}^{\text{local}}$ to the increase of ECSA with relative humidity. A mixture of both contributions is expected to hold in practice.

The reduction of $R_{O_2}^{\text{local}}$ with temperature can be fundamentally explained by the thermal activation of oxygen transport, so that there is an increase of the effective diffusivity and adsorption rate coefficients of oxygen (Shen et al., 2017; Conde et al., 2019; Yakovlev et al., 2021). In addition, rising temperature at constant relative humidity increases the partial pressure of water, which can in turn increase the volume fraction of water in the ionomer (Shen et al., 2017).

The adverse effect of pressure on $R_{O_2}^{\text{local}}$ is unexpected but can be understood based on the adsorption kinetics at the gas/ionomer interface (Shen et al., 2017; Garsany et al., 2018; Sun et al., 2020; Yakovlev et al., 2021). As discussed by Shen et al. (Shen et al., 2017), according to Eq. 7, $R_{O_2}^{\text{local}}$ increases with oxygen concentration and therefore pressure due to saturation of the adsorption rate of oxygen at the gas/ionomer interface. It is worth noting that the effect of pressure cannot be explained by means of linear Henry's law, so oxygen isotherms with a concave shape are needed, such as Langmuir-type isotherms.

2.2 Effect of ionomer content and morphology

The concentration and morphology of the ionomer play a key role on $R_{O_2}^{\text{local}}$ due to the kinetic effect of ionomer on local oxygen

transport above and beyond operating conditions and water saturation (Cheng et al., 2022a). In particular, many previous studies focused on the effect of ionomer-to-carbon weight ratio, I/C [34, 38, 39], and equivalent weight of ionomer, EW [33, 35, 40, 41] (see Figure 4). Results showed an overall increase of $R_{O_2}^{\text{local}}$ with I/C [34, 38, 39]. However, opposite trends have been observed for EW [33, 35, 40, 41]. The fitted expressions for $R_{O_2}^{\text{local}}$ (I/C) and $R_{O_2}^{\text{local}}$ (EW) are given by

$$R_{O_2}^{\text{local}} = 0.11 \exp(1.92I/C) \text{ s cm}^{-1} \quad (9.1)$$

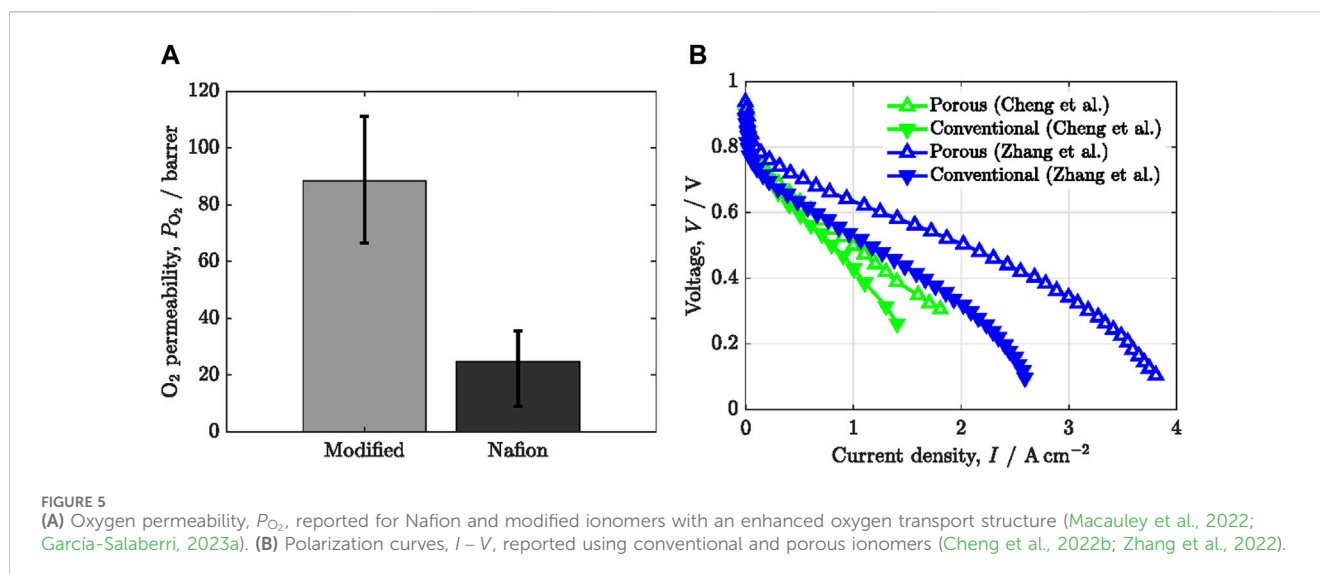
$$R_{O_2}^{\text{local}} = -0.06 + 1.6 \times 10^{-4} EW \text{ s cm}^{-1} \text{ (increasing)} \quad (9.2)$$

$$R_{O_2}^{\text{local}} = 0.19 - 7.25 \times 10^{-5} EW \text{ s cm}^{-1} \text{ (decreasing)} \quad (9.3)$$

where EW is expressed in SI units.

The detrimental effect of I/C on $R_{O_2}^{\text{local}}$ is mainly caused by two factors: i) increase of average ionomer thickness with ionomer content, and ii) increase of agglomeration caused by ionomer maldistribution at exceedingly high volume fractions (Wang et al., 2019; Sun et al., 2021). These two effects are expected to manifest when I/C is varied in a wide range between $I/C \approx 0.1$ and $I/C \approx 1$. However, for intermediate values around $I/C \approx 0.6$, it is possible that an increase of the ionomer content enlarges the ECSA due to the coverage of previously inactive catalyst areas. Hence, ionomer thickness and ionomer agglomeration do not have a noticeable effect, so that $R_{O_2}^{\text{local}}$ remains rather invariant or even decreases, as shown by Yakovlev et al. (Yakovlev et al., 2021).

A decrease of EW leads to an increase in the number of protogenic groups in ionomer, so that water uptake and ionic conductivity are typically promoted (Kusoglu and Weber, 2017; García-Salaberri, 2023a). The higher water volume fraction and shorter side chains in ionomer facilitates oxygen transport through ionomer, leading to a decrease of $R_{O_2}^{\text{local}}$. This scenario has been previously observed experimentally by several authors, either examining the local or total oxygen transport resistance (Garsany et al., 2018; Ramaswamy et al., 2021). However, other authors have reported an opposite behavior (Ono et al., 2013; Poojary et al., 2020). The explanation provided by these authors relies on the



arrangement of water rather than the amount of water in the ionomer. According to Poojary et al. (Poojary et al., 2020), an increase of EW locates water uptake preferentially at the Pt/ionomer interface. Consequently, the diffusive tortuosity is reduced due to a better distribution of oxygen over the catalyst surface. Note that the limiting transport process at the local scale has been previously ascribed to the formation of a dense ionomer layer near the catalyst surface (Jinnouchi et al., 2016; Kurihara et al., 2017; Kurihara et al., 2019). According to Ono et al. (Ono et al., 2013), enhanced water uptake at decreased EW may be mainly concentrated at the gas/ionomer interface, resulting in an exceedingly high coverage of water on the ionomer and much lower oxygen concentration in the ionomer. Another plausible explanation introduced here is the poisoning effect of sulfonic groups on the Pt surface in low- EW ionomers, which can lead to an ECSA reduction and therefore an increase of $R_{O_2}^{local}$. Further work is needed to elucidate the interplay between $R_{O_2}^{local}$, ECSA and oxygen transport in water as a function of EW .

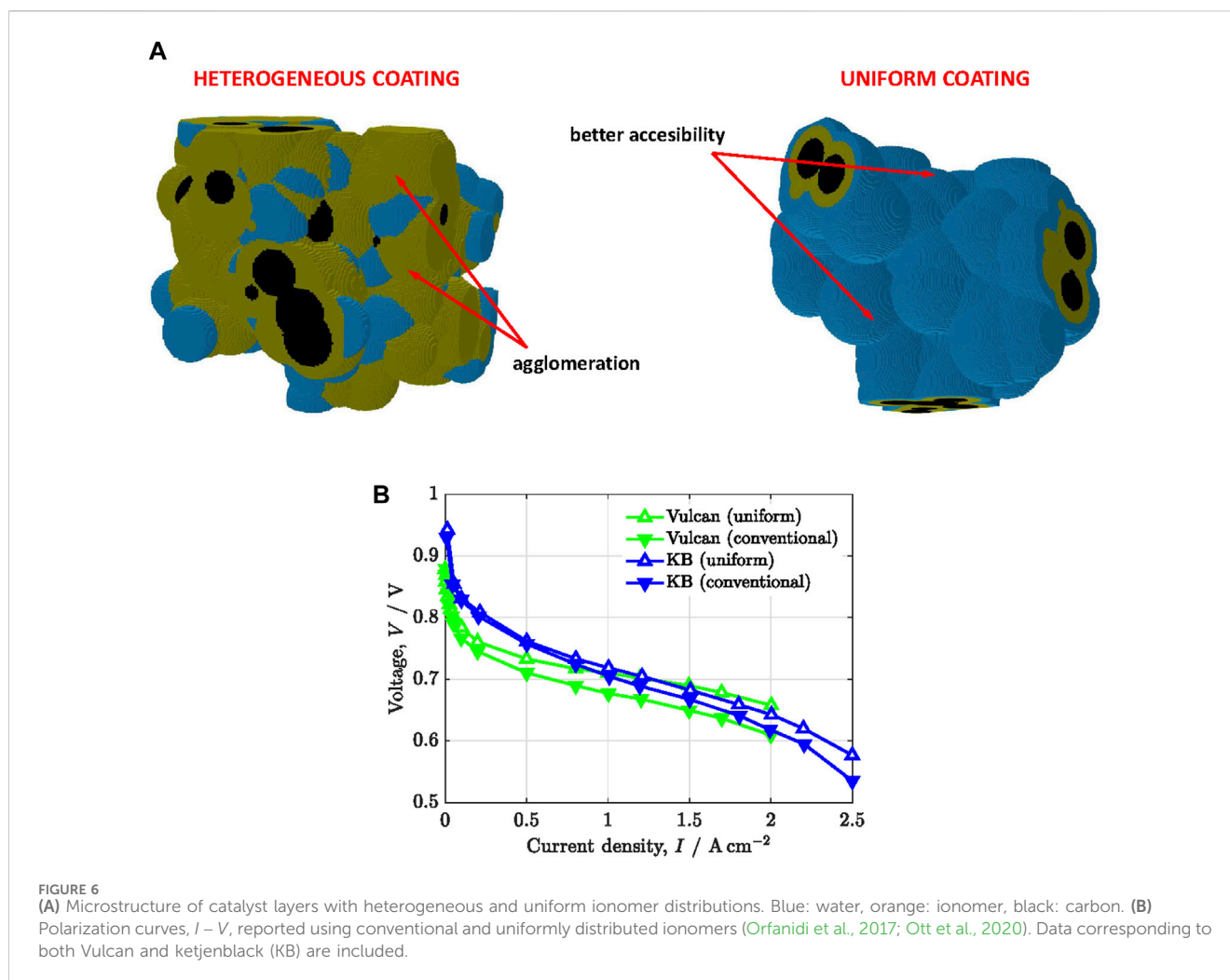
Increasing oxygen permeability by modification of ionomer chemical structure provides a straightforward approach to reduce $R_{O_2}^{local}$. Figure 5A shows the oxygen permeability of Nafion compared to that of modified ionomers examined by Macauley et al. (Macauley et al., 2022). An increase of oxygen permeability up to a factor of 5 was achieved in (Macauley et al., 2022), while preserving good proton conductivity, using copolymers with blocks designed to enhance both oxygen and proton transport. Improved oxygen permeation was reached by means of an open-ring polymer structure, which led to a decrease of $R_{O_2}^{local}$ down to a factor of 2 and peak power densities higher than 1.25 W cm^{-2} ($L_{Pt} = 0.1 \text{ mg}_{Pt} \text{ cm}^{-2}$). In addition, durability was improved, exceeding the target set by the U.S. Department of Energy at 0.8 A cm^{-2} . The enlarged durability was explained by a more uniform ionomer distribution compared to Nafion, along with lower levels of Pt particle size growth and ionomer degradation.

The design of porous ionomers is also a powerful approach, as an alternative to the modification of ionomer chemical structure (Cheng et al., 2022b; Zhang et al., 2022). Recently, Cheng et al. (Cheng et al., 2022b) developed nanoporous ionomers by regulating

the nanoscale distribution of Nafion using a sacrificial pore-forming agent. The introduction of nanoporosity on/in Nafion films significantly increased the number of triple-phase points for oxygen reduction reaction (ORR) and decreased $R_{O_2}^{local}$ by around one order of magnitude compared to conventional Nafion (0.08 s cm^{-1} vs 0.37 s cm^{-1} at $L_{Pt} = 0.1 \text{ mg}_{Pt} \text{ cm}^{-2}$). As a result, a markedly superior performance was achieved at high current density, as shown in Figure 5B. In another work, Zhang et al. (Zhang et al., 2022) synthesized mesoporous ionomer films by incorporating ionic covalent organic framework (COF) nanosheets into Nafion (pore size $\sim 3\text{--}4 \text{ nm}$). The use of COF-modified ionomer resulted in a two-fold decrease of $R_{O_2}^{local}$ and a reduction of the poisoning effect of sulfonic groups on the Pt surface, showing higher catalyst mass activity and ECSA. Consequently, as shown in Figure 5B, the peak power density was improved by a factor of 1.6 using the mesoporous ionomer with both pure oxygen and air feed ($L_{Pt} = 0.07 \text{ mg}_{Pt} \text{ cm}^{-2}$).

2.3 Effect of ionomer distribution on catalyst particles

Apart from ionomer thickness, the ionomer distribution on the carbon support plays an important effect on local oxygen transport. In the last years, several researchers have investigated the use of functionalized carbon supports with nitrogen-containing surface groups to tailor ionomer distribution (Orfanidi et al., 2017; Ott et al., 2020). Orfanidi et al. (Orfanidi et al., 2017) examined the performance of animated Vulcan compared to conventional non-functionalized carbon supports at low Pt loading ($L_{Pt} = 0.07 \text{ mg}_{Pt} \text{ cm}^{-2}$). The interaction between positively charged groups of carbon support and negatively charged groups of ionomer led to a more uniform ionomer distribution. As illustrated in Figure 6A, the higher uniformity of ionomer films prevented agglomeration and the formation of deactivated ionomer-free regions. Consequently, an optimal balance was achieved between ionic and mass transport losses, increasing performance at low Pt loading (see polarization curves with Vulcan in Figure 6B) (García-



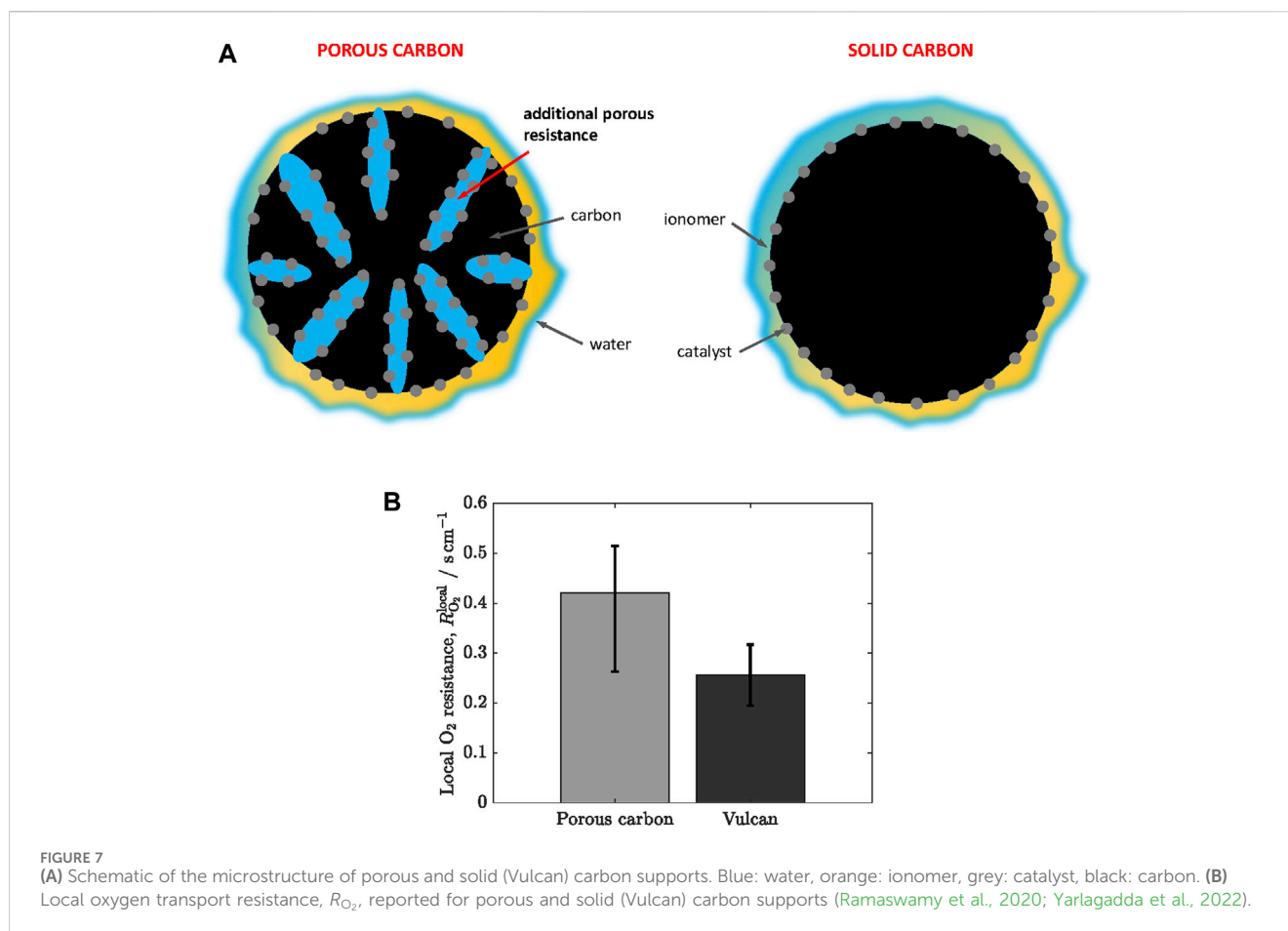
Salaberri, 2023b). Besides, it is worth noting that the optimal I/C was reduced from $I/C \approx 0.65$ for the conventional electrode down to $I/C \approx 0.4$ for the functionalized electrode. The reduction can be explained by the more uniform ionomer distribution and the better Pt/C coverage achieved on the functionalized carbon surface. A similar research approach was presented by Ott et al. (Ott et al., 2020) but using porous ketjenblack (KB) instead of non-porous Vulcan. As shown in Figure 6B, improved performance was also achieved at low Pt loading ($L_{Pt} = 0.11 \text{ mg}_{Pt} \text{ cm}^{-2}$) due to a proper balance between reduced mass transport losses and good ionic conductivity. The combined results of Orfanidi et al. (Orfanidi et al., 2017) and Ott et al. (Ott et al., 2020) show that the positive effect of ionomer uniformity does not depend on the porosity of the carbon support.

2.4 Effect of carbon porosity

Two types of carbon supports are commonly used depending on their porosity: i) Vulcan or solid carbon with virtually no porosity, and ii) high surface area, micro/mesoporous carbon, such as ketjenblack. Previous work has shown that local oxygen transport is dependent on the location of catalyst nanoparticles in the carbon support. As shown

in Figure 7A, the solid surface of Vulcan allows an external location of Pt nanoparticles, while ketjenblack shows catalyst nanoparticles both in the inner micro/mesopores and the external surface. Usually, most of the nanoparticles in porous carbon are located in the inner surface (>60%) (Padgett et al., 2018). Harzer et al. (Harzer et al., 2018) tuned the preferential location of Pt nanoparticles in ketjenblack by varying the synthesis method. They found that $R_{O_2}^{local}$ decreased when most of the nanoparticles were located on the outer surface due to suppression of the additional transport resistance introduced by (partially) saturated micro/mesopores. As shown in Figures 7A,B similar conclusion can be extracted from the works of Ramaswamy et al. (Ramaswamy et al., 2020) and Yarlagadda et al. (Yarlagadda et al., 2022), who tested a wide variety of porous carbon supports. Theoretically, Darling and Burlatsky (Darling and Burlatsky, 2020) developed a nanoscale model for the oxygen transport resistance in ketjenblack, which was validated against experimental data. Two main factors were identified for the enlarged oxygen resistance in porous carbon: i) a higher entry loss through ionomer at pore mouth, and ii) oxygen diffusion in the (partially) saturated micro/mesopore.

Despite the increase of $R_{O_2}^{local}$ usually found in porous carbon supports, it is worth noting that they have the beneficial effect of increasing the catalyst activity due to suppression of the poisoning effect of ionomer sulfonic groups on catalyst sites. Therefore, a



proper design of the micro/mesopore carbon structure can be a suitable approach to improve kinetics while ensuring a relatively low local oxygen transport resistance. The generation of accessible and short nanopores in carbon with a virtually negligible ionomer coverage is preferred, so that the local transport resistance is lowered in a similar way to that of nanopores introduced in mesoporous ionomers (Cheng et al., 2022b; Zhang et al., 2022). This approach has been recently shown by researchers from General Motors to boost the performance of low Pt-loading PEFCs (Yarlagadda et al., 2018). They optimized porous carbon support by increasing the volume fraction of accessible mesopores for both proton and oxygen transport in the range between 4–7 nm.

2.5 Additional factors

Other aspects that have shown a significant influence on $R_{O_2}^{local}$ include: i) dispersion of Pt nanoparticles on carbon support, ii) oxygen accessibility in primary pores of agglomerates, and iii) pore morphology of the catalyst layer.

The effect of Pt dispersity was examined by Sun et al. (Sun et al., 2020) using catalyst layers with constant thickness and different Pt-to-carbon weight ratios, *wt*. Catalyst dispersity was reduced by gradually increasing *wt*. A significant improvement in performance at high current density was found in catalyst layers with low dispersity

($L_{Pt} \approx 0.1\ mg_{Pt}\ cm^{-2}$). The positive effect of decreasing catalyst dispersity can be understood by a reduction of the diffusive transport length through ionomer and water films from the bulk pore space toward the Pt surface. The effect of oxygen accessibility in primary pores was examined numerically and experimentally by Cetinbas et al. (Cetinbas et al., 2020) and Garsany et al. (Garsany et al., 2018), respectively. These works showed that increasing microporosity can enhance water evaporation, thereby reducing flooding in primary pores (Garsany et al., 2018). Achieving high oxygen accessibility in primary pores by flooding reduction is critical to ensure the facilitated transport of oxygen through agglomerates under fully humidified conditions (Cetinbas et al., 2020). In addition, the arrangement of pores and not only the porosity of the catalyst layer plays a crucial role in promoting local oxygen transport around ionomer films. For example, vertically aligned microstructures can maximize oxygen accessibility through the bulk pore space, while minimizing interaction and agglomeration between adjacent ionomer films (Murata et al., 2014; García-Salaberri, 2023b). The effect of assembly compression on the microstructure of the catalyst layer is minor at moderate pressures below 1.5 MPa but can originate significant changes at high pressures around 3–5 MPa (Sassin et al., 2016; Malekian et al., 2019). Excessive compression of the catalyst layer leads to a decrease in large secondary pores, reducing the average pore size and the porosity of the catalyst layer (Malekian et al., 2019). In addition, membrane swelling can form cracks in the catalyst layer (Kai et al., 2014). The morphological changes of the

TABLE 3 Summary of transport processes in the electrode of a PEFC.

N°	Species	Process	Medium characteristics
1	O ₂	Molecular diffusion	Large free pores partially saturated with water
2	O ₂	Knudsen diffusion	Small free pores, partially saturated
3	O ₂	Transport through ionomer	Ionomer film hydrated
4	O ₂	Transport through liquid water	Water film interacting with particles and/or ionomer
5	O ₂	Surface diffusion over catalyst particles	Surface around catalyst centers
6	H ⁺	Grothuss mechanism	Bulk liquid water partially saturating pores
7	H ⁺	Transport inside ionomer film	Ionomer channel structure saturated with water
8	H ⁺	Surface diffusion over catalyst particles	Particles surface around catalyst centers
9	H ₂ O (l)	Capillary transport	Free pores partially saturated with water
10	H ₂ O (g)	Molecular diffusion	Free pores partially saturated with water
11	H ₂ O (ionomer)	Diffusion	Ionomer channel structure in CL and membrane
12	H ₂ O (lg)	Dragging	Flow field channel
13	e ⁻	Bulk and surface transport	Solid particles and interparticle space

catalyst layer caused by mechanical stresses can affect local flooding and oxygen accessibility toward Pt sites.

3 MEA design and mitigation strategies

As discussed in previous sections, at intermediate and high current densities, mass transport resistances limit power production in a PEFC. Different transport processes are responsible for these resistances, and involving different species, as summarized in Table 3. This part of the revision will provide some experimental strategies proposed recently for the mitigation of transport resistances associated with some of the processes in Table 3, especially those involving local oxygen mass transport in the porous media of the electrodes which correspond to processes 3, 4 and 5 of Table 3. A conventional PEFC electrode structure will be assumed, having three serial porous layers, namely, the gas diffusion layer (GDL), microporous layer (MPL), and catalyst layer (CL).

Among the different processes in Table 3, of special importance is the transport of liquid water inside the pore structure of the electrodes (processes 9 and 10) due to the large impact on other transport processes of O₂, H⁺, e⁻ and on the electrochemical kinetics (Li et al., 2008; Das et al., 2010; Iranzo et al., 2016; Lübber et al., 2023). The slowness of water transport, which is dominated by capillary forces in the porous layers of the MEA (Gostick, 2013; Mulone and Karan, 2013; Zapardiel and García-Salaberri, 2022), makes an important contribution to the transport resistances in a PEFC. Water is the product of the ORR in the cathode and provides the medium for the ionic transport in the CLs and the membrane; on the other hand, liquid water in flooded pores becomes a barrier for the access of gas molecules to the catalytic centers obliging the dissolution and diffusion of gas molecules into the liquid, which is four orders of magnitude slower than their diffusion in the free pore space.

Another important source of mass transport resistance in a PEFC is the local access of gas molecules to the reaction sites, principally oxygen in the cathodic CL, understanding for 'local' the nanometric scale comprising the ionomer thickness and the catalyst particle, corresponding to processes 3, 4 and 5 in Table 3 (see Figures 2, 8). Since the Pt surface must be closely interacting with the proton conductor, i.e., the ionomer phase, this same phase may cause partial blockage of the reaction sites that is revealed as a mass transport resistance. The problem is especially severe at low Pt loadings in the CL since such 'local transport resistance' depends on the inverse of the CL thickness (Pt loading) (Schuler et al., 2019).

Therefore, the reduction of mass transport resistance in a PEFC concerns actuations at different scales in the MEA. On the one hand, the management of liquid water in porous layer requires its removal at the highest rate but leaving steady partially saturated pores to preserve ionic conduction. Most strategies to achieve this ideal situation rely on tuning the hydrophilic-hydrophobic properties of the pore walls and appropriate ionomer distribution (Figure 8B) able to keep partially saturated pores in the CL and to favor capillary transport and water diffusion. New electrode structures have also been envisaged to favor transport processes (Schuler et al., 2019). At the same time, mass transport at the local, nanoscale level, very close to the reaction sites, must be accelerated which should address the local reaction environment and the ionomer distribution to allow fast simultaneous accessibility of protons and gas molecules (cf. Figures 8C,D).

Some recent strategies to improve mass transport properties are described below.

3.1 Mass transport resistance mitigation

The strategies for mass transport improvement in a PEFC can be classified into three types regarding different scales in an MEA:

- a) Materials of porous layers (GDL, CL, MPL).

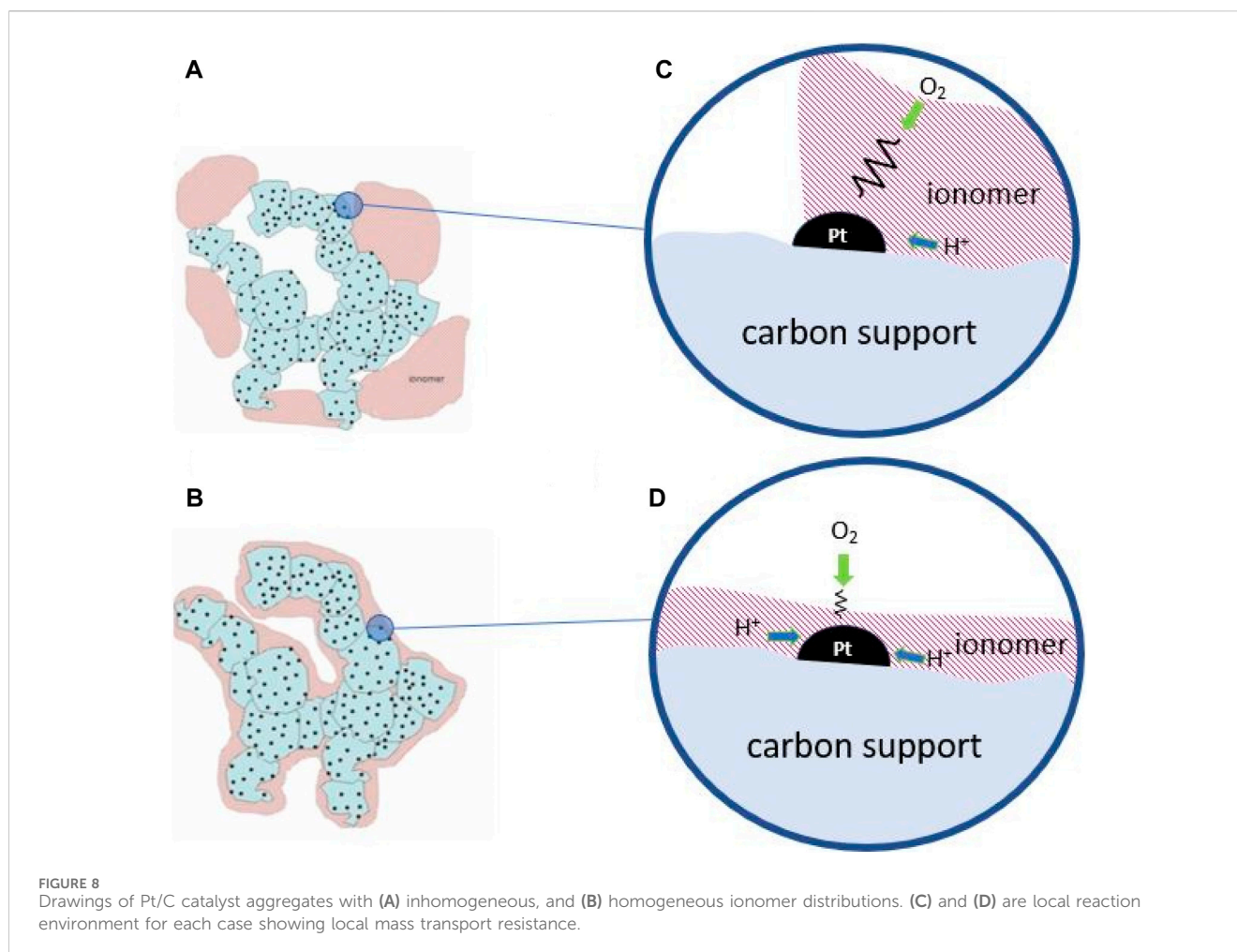


FIGURE 8
Drawings of Pt/C catalyst aggregates with (A) inhomogeneous, and (B) homogeneous ionomer distributions. (C) and (D) are local reaction environment for each case showing local mass transport resistance.

- b) Structure of the porous layer and fabrication process.
- c) Membrane-electrodes assembly configuration.

Actuations at one level may have an impact on transport at the other levels, as well as on materials costs, performance, and cell durability. Their implementation should be preceded, therefore, by a comprehensive analysis including the different aspects.

3.1.1 Materials of the porous layers

Carbon materials. Microporous carbon particles make up the larger proportion of the electrode mass, so it should not be surprising that their properties have a large impact on transport processes. Its surface chemistry governs the interaction of water in the porous layers through polar substituents that provide variable hydrophilicity (Shen et al., 2008; Khodabakhshi et al., 2020), whereas porosity and pore size distribution have strong effects on proton conduction, ORR kinetics, and electrode durability (Uchida et al., 1995a; Liu et al., 2011a). The surface composition of carbon can be modified before the electrode preparation to tailor water interaction properties.

Enhancing the hydrophobic character of carbon surface, i.e., decreasing wettability, has been shown to improve, in general, liquid water transport (McNeary et al., 2020). Among different treatments, thermal and chemical treatments are

preferred for surface modification (Shen et al., 2008). Thermal treatments in inert atmospheres or H₂, decrease the number of polar surface groups and increase hydrophobicity, which is beneficial for water transport in the CL, MPL and GDL. Another means to provide hydrophobic character to the porous carbon structure is by adding hydrophobic agents. The most used is PTFE (Teflon), which is normally applied to the MPL and GDL. It has also been used inside the CL, however, here it has negative impacts on other properties, like electrical conductivity, porosity, and ECSA (Avcioglu et al., 2015). As a consequence, PTFE has been applied to the CL together with other treatments. Hydrophobic and porosity of the CL and MPL were tested by Mohseninia et al. (Mohseninia et al., 2020) using PTFE and pore formers, respectively, and water accumulation followed *in situ* with the neutron tomography technique. The results showed that a high hydrophobicity of the cathodic MPL increases water flooding and decreases performance, whereas more porous layers provide superior performance at high current density with oxygen transport occurring through small pores and water through larger pores. A new method for hydrophobization of a porous layer, without adding new chemicals to the preparation process, is by using the electrospray deposition technique that will be described in the next section (Conde et al., 2021).

Certain strategies to improve water transport in the electrode are based on a combination of hydrophilic and hydrophobic treatments to induce different water interactivity in different parts of the electrode, which could accelerate water drainage (Roh et al., 2018). With this aim, hydrophilicity is enhanced with acidic treatments, like using nitric or sulfuric acid, which results in partial surface oxidation due to an increase in the amount of oxygen polar groups (Shen et al., 2008). A similar effect can be obtained from a thermal treatment in an oxidative atmosphere. Mild hydrophilicity can be attained by catalyst treatments with soft chemicals, which improves ionomer dispersibility and is beneficial for PEFC performance (Nagamori et al., 2023). However, the hydrophilic character of the carbon surface is normally a result of PEFC operation under stressing conditions (like start-up and shut-down), which favors flooding and lower interparticle electric contact leading to a decrease in performance, so it becomes one principal cause for PEFC aging (Borup et al., 2020).

Together with surface chemistry, the structure and morphology of the carbon material have an influence on transport properties in the CL. The size of grain aggregates, the microporosity, or the total area may change water interaction and, with it, transport properties in the porous layers (Uchida et al., 1995a; Uchida et al., 1996). These parameters are also related to other important aspects, like chemical stability, catalyst particle interaction, and electrical conductivity, so their selection must be carried out on a general optimization plan. Hence, the synthesis method of the Pt/C catalyst may determine the transport resistance, since Pt particles may be distributed in different locations over the carbon surface, with different accessibility. Pt particles inside nanopores are prone to have better catalytic activity but poorer oxygen mass transport (Harzer et al., 2018) (see Figure 7).

Primary pores and surface chemistry of the carbon phase govern Pt growth during Pt/C synthesis, and properties, like particle size, dispersion, and location. Growth inside carbon micropores may lead to poorly accessible Pt and important losses due to mass transport and electrochemical surface area availability (Iden et al., 2013b). Such effect has been recently studied on high performance electrodes, like those used for the Toyota Mirai fuel cell, showing that primary pores with limited accessibility determine local oxygen transport resistance, as well as the ionomer phase characteristics (Cetinbas et al., 2020). The latter is a result of the interaction of the ink with the carbon surface (Liu et al., 2011b; Uchida, 2020; Woo et al., 2020; Cheng et al., 2021) and the deposition process as will be discussed below.

Certain nanostructured carbon materials may favor the transport properties of electrodes and catalysis when they have a stable and uniform decoration with Pt nanoparticles (Sharma and Pollet, 2012; Zhu et al., 2013). Nanofibers and nanotubes (single and multi-walled) have been extensively studied in this sense, and have accomplished important technical targets for the PEFC technology (Jha et al., 2013). Such carbon morphologies favor a decrease in the tortuosity and in the interparticle connection resistances, leading to improved mass transport (molecular and Knudsen diffusion), as well as better ionic and electronic conductivities of the CL (Kannan et al., 2007; Vairavapandian et al., 2008). To our knowledge, the effect on the local oxygen transport resistance is less studied. Graphene and graphene oxides as Pt support provide large electrochemical surface area and stability, but mild improvements in PEFC performance have been obtained so far compared with

carbon blacks (Daş et al., 2017; Işikel Şanlı et al., 2017; Grigoriev et al., 2018; Kim et al., 2019).

Ionomer phase. The ionomer is the component of the CL that, upon absorption of liquid water in its polymeric structure, generates an aqueous path for proton conductivity within the CL. It has other roles, like surfactant in the catalytic ink, and particle binder in the CL (Kusoglu and Weber, 2017). Most ionomer chemistries contain a backbone perfluorinated chain with acidic groups in side-chains, normally sulfonic (-SO₃H), that are responsible for water interaction and ionic conductivity. Of special impact on transport properties is the ionomer distribution and configuration within the CL, and the interaction of sulfonic groups with Pt surface. An additional oxygen transport resistance arises because of the ionomer phase close to Pt sites, called 'local mass transport resistance', which has an important impact on performance especially when trying to decrease the catalyst loading in the CL (Sun et al., 2023) (see Figure 8).

Different strategies have been proposed to mitigate such ionomer-induced mass transport resistance. The use of hydrophobic agents, C₁₆HS, during CL deposition was attempted by Sun et al. (Sun et al., 2023) to reduce the sulfonic group interaction with Pt, leading to an important increase in performance in rotating disk electrode (RDE) and single-cell studies. Orfanidi et al. (Orfanidi et al., 2017) changed the distribution of the ionomer in the CL by introducing nitrogen-containing surface groups on the carbon support surface. The procedure led to a decrease in the pressure-independent oxygen transport resistance of the layer, which is the resistance due to transport within the ionomer film and related to the local transport resistance. Changing the ionomer chemistry is another way to mitigate the interaction of sulfonic groups with Pt. Rolfi et al. (Rolfi et al., 2018) attained a 20% increase in oxygen permeability that gave rise to lower mass transport resistance, by using a modification of Aquivion with a steric hindered monomer. Garsany et al. (Garsany et al., 2018) observed a decrease in the resistances of proton transport, oxygen transport, and charge transfer when changing from an ionomer with a long side chain, like Nafion, to a shorter side chain like Aquivion.

3.1.2 Structure of the porous layer and fabrication process

The morphology of the porous layers, especially the CL, has a major impact on water management in the cell (Litster and McLean, 2004; Conde et al., 2019; Chen et al., 2020; Liu S. et al., 2023; Tempelaere et al., 2023). Morphology is characterized by several parameters, including agglomerate size, secondary pore size and density, thickness, and tortuosity. The first principle numerical simulation shows that better transport properties and high performance in the CL require high porosity and low tortuosity in the CL (García-Salaberri, 2023b).

Strategies to improve the morphology address principally the procedure used for the porous layer deposition. Most used preparation methods, and closer to large-scale electrode manufacture, are those based on the deposition of a suspension ('ink') of the catalyst and the ionomer in a solvent, to produce a thin, porous film (Litster and McLean, 2004). By these means, different film properties can be obtained depending on the suspension chemistry, deposition parameters, and substrate.

The ink properties have an impact on the resulting morphology of the porous layer. Suspension chemistry mostly concerns the solvent and concentrations of particles and ionomer, which determine the stability of the suspension, their mutual interactions, and the state of the ionomer in the ink (Uchida et al., 1995b; Berlinger et al., 2021; Guo et al., 2021). The latter governs distribution and morphology within the deposited catalyst layer, and, ultimately, secondary pores (meso and microporosity) and transport properties. A solvent with a high dielectric constant favors the dissolved ionomer state, i.e., isolated chains fully interacting with the solvent, whereas decreasing values will favor their aggregation towards colloidal and solid particle states. However, the effect of the dielectric constant on catalyst layer morphology is unclear (Berlinger et al., 2021). The interaction of the ionomer with the particles in the ink is a matter of numerous studies since it will determine CL morphology and component distribution in ink deposition by spray coating (Berlinger et al., 2021).

The substrate used for CL deposition has also an influence on porous layer morphology and transport properties. For CL deposition, the MPL or the membrane can be used, or an external substrate to transfer the CL to the MEA (decal method) (Cho et al., 2009). Easier experimental handling results from using the MPL, where deposition can be carried out at different scales and using fast techniques, like spray coater in automatic roll-to-roll configurations, so it is probably preferred in commercial products ('catalyst covered GDLs'). The deposition on the membrane is experimentally more difficult due to the management of the hydrophilic polymer membrane when receiving the sprayed ink, which may crease easily and become damaged by solvent absorption and reactivity. On the other hand, it is demonstrated that on-membrane deposition provides better ionic contact between the membrane and the CL, which results in an important reduction of the cell's internal resistance (Chaparro et al., 2011). To proceed with this strategy, decal methods have the advantage of using a sacrificial substrate where the solvent can be eliminated before transferring the CL to the membrane. A different option for on-membrane deposition is using a 'dry ink deposition method', like electro-spray (Chaparro et al., 2011). In addition, electro-spray results in new CL transport properties that mitigate transport resistances as described below.

The ink deposition method is very determining for the CL morphology and transport properties. Ink deposition methods have been used in different types, from pure impregnation (Benítez et al., 2005), to airbrushing or ultrasonic spray (Jao et al., 2013; Turtayeva et al., 2022), ink-jet (Shukla et al., 2014), roll-to-roll (Liu P. et al., 2023), electrospinning (Brodt et al., 2015), and electro-spray deposition (Martin et al., 2010; Takahashi et al., 2016; Folgado et al., 2018; Cho et al., 2020; Yoshino et al., 2020; Conde et al., 2021). Impregnation and spray coating techniques are widely used due to their fast deposition rate, easier experimentation and availability of commercial equipment that can be used for laboratory work and large-scale electrode production. Their main drawbacks are poor film morphology control and reproducibility, which depends on careful ink preparation and coating equipment, notwithstanding personnel experience and skills. It may have low catalyst yield deposition, especially in small areas, leading to the waste of expensive material (platinum and ionomer) and an increase

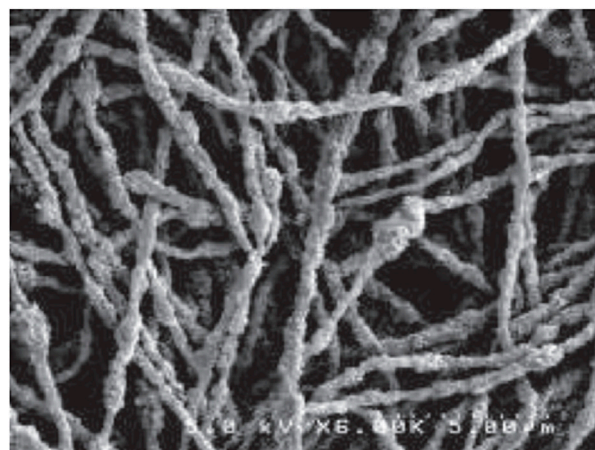
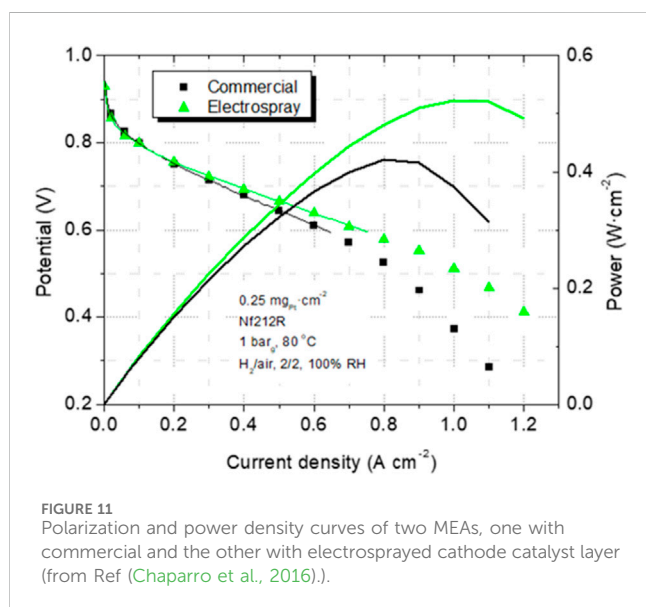
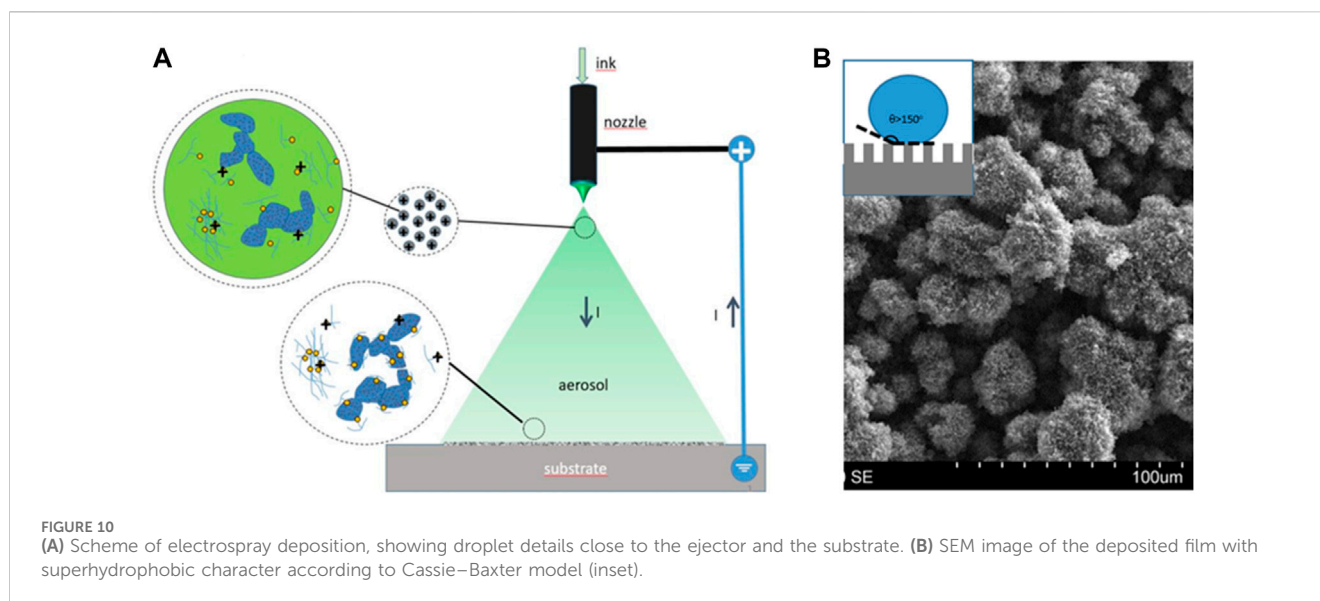


FIGURE 9
SEM image of an electrospun nanofiber mat. From Ref. (Brodt et al., 2015).

in costs. Ink-jet technology like used in commercial printers has been applied to improve process reproducibility and yield, but with a minor impact on film transport properties (Shukla et al., 2014).

Different CL morphology and transport properties are obtained by using electrospinning and electro-spraying deposition techniques. Both are based on spraying the catalytic ink under the influence of a strong electric field, which is an additional parameter for the control of the deposition process. Under the electric field, droplet ejection may result in the growth of a thin filament or the generation of a progeny of droplets, due to the opposing effects of Coulomb repulsion and surface tension. In the first case, electrospinning deposition occurs with the formation of microwires of the catalyst and the ionomer that improve connectivity among particles, oxygen accessibility and water transport properties of the films (Brodt et al., 2015) (see Figure 9).

The electro-spray deposition occurs when Coulombic and surface tension opposing forces favor the fission of the ejected droplets (Figure 10), which gives rise to completely different CL morphology and transport properties (Folgado et al., 2018; Conde et al., 2019; Conde et al., 2021). During electro-spray, the fission of ink droplets in-flight, after ejected, accelerates solvent evaporation, favoring catalyst and ionomer particles arrival at the substrate free of solvent ('dry deposition') (see Figure 10A). This makes a substantial difference compared with other ink deposition techniques. Dry catalyst particles and ionomer are deposited under the influence of electrostatic and image forces instead of ink interactions governing spray deposition, which results in a particular porous morphology (Higuera, 2018). The accommodation of particles and the ionomer gives rise to a macroporous and dendritic structure that renders superhydrophobic pores walls (Cassie-Baxter type) (see Figure 10B). Electro-spray is very appropriate for deposition on membrane substrate due to the arrival of particles without solvent, yielding lower CL-membrane contact resistivity (Chaparro et al., 2011). Transport is enhanced in electro-sprayed layers due to their more homogeneous ionomer distribution (Figures 8B,D). Local oxygen transport is also favored by the probably different ionomer structure and local reaction



environment around catalyst sites, as reflected by a significant reduction in the local transport resistance (Conde et al., 2019), and improvement in fuel cell response (see Figure 11) (Chaparro et al., 2016). The characteristics of the electro sprayed ionomer structure and local reaction environment are a matter of present research. Electro spray properties also concern electrode's durability and material costs (Conde et al., 2021), which increase the interest for the industrial manufacture of PEFC electrodes.

Apart from using different ink deposition methods, different CL structures may be obtained with improved transport properties by other means. Including ordering and 3D structuring in the CL has shown a positive impact on mass transport properties and catalyst utilization, as highlighted in a recent review (Tempelaere et al., 2023), due to a decrease in tortuosity and enhanced Pt accessibility in ordered structures. Ordering in CL relies on more involved synthesis and deposition processes, compared with ink deposition, which must be

comprehensively analyzed if attempting the transfer from laboratory to industrial fabrication. Carbon nanotubes have been vertically aligned over the membrane surface, and MEAs of up to 236 cm² have been tested with showing exceeding performance beyond US-DOE targets for Pt mass activity (Yarlagadda et al., 2018). The alignment is a result of a carbon deposition on a sacrificial substrate (stainless steel), followed by Pt and Nafion depositions, and a decal transfer to the membrane. Ordered CLs of microscale arrays of Pt/C disks, and arrays of holes on Pt/C films, have been prepared by lithographic technique, leading to improvements in water transport and mass activity in single PEFC, but having crossover and short-circuiting issues caused by the inherent compression inhomogeneities (Paul et al., 2020). Introducing profiles in parameters of the CL, like ionomer and catalyst concentration, normally in the through plane direction, has also been demonstrated to improve transport properties. In this case, the effect favors gradient forces for water transport, like capillary-driven flow and phase-change induced transport, leading to a reduction of mass transport losses (Cetinbas et al., 2014; Chen et al., 2017; Nguyen et al., 2022).

3.1.3 Membrane-electrodes assembly configuration

At the MEA level, an appropriate combination of anode and cathode properties may maximize water gradients and accelerate water transport and removal. With this aim, different combinations of CLs have been tested in single PEFCs, and their water management studied (Folgado et al., 2018). The use of superhydrophobic CLs in the cathode in front of hydrophilic CLs in the anode has shown enhancement of water transport from the cathode to the anode (see Figure 12). This configuration favors high anode humidification and avoids cathode flooding at high current densities, which gives rise to a notable increase in peak power density, above 20% compared with standard, symmetrical, configurations where cathode and anode have similar hydrophilicity (Figure 11). On the other hand, the reverse case, i.e., a superhydrophobic anode in front of a hydrophilic cathode, increases the possibility of severe membrane drying close to the anode and its damaging. These results are valid for self-humidified

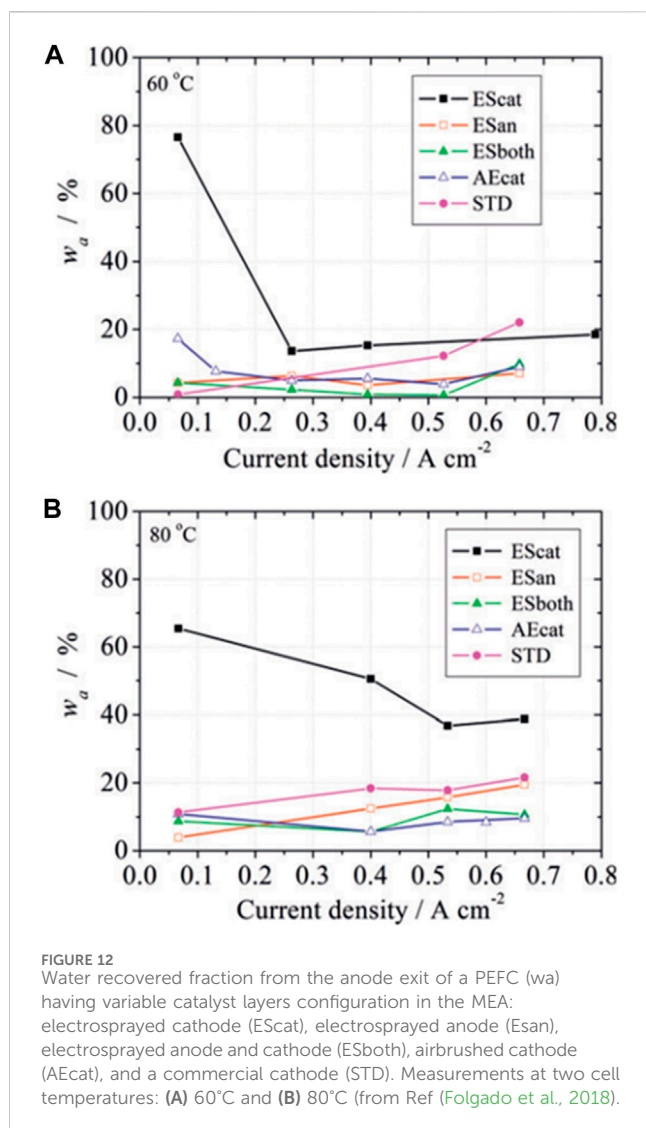


FIGURE 12
Water recovered fraction from the anode exit of a PEFC (w_a) having variable catalyst layers configuration in the MEA: electrosprayed cathode (EScat), electrosprayed anode (ESan), electrosprayed anode and cathode (ESboth), airbrushed cathode (AEcat), and a commercial cathode (STD). Measurements at two cell temperatures: (A) 60°C and (B) 80°C (from Ref (Folgado et al., 2018)).

cell operation under rather common excess flow rate stoichiometry H_2/O_2 of 1.5/3.0 in anode and cathode.

The optimal MEA configuration must take into account the operating conditions in a PEFC. For example, two radically different operating conditions are the *convective* and the *passive feeding* in a PEFC. The first is the conventional operation mode where reactant gases are kept flowing parallel to the electrode plane to accelerate the transport of water and removal from the cell. This mode requires additional system components to keep the flow regimes and allows for high power production. On the other hand, the passive feeding mode does not require forced convection of gases but relies on passive forces for transport processes: capillarity, diffusion, evaporation, gravity, and natural convection. A passive PEFC has an air-breathing cathode in contact with ambient air, and a dead-end anode, where water transport rates are typically lower than in a convective cell, as well as the power attained, but the system is simpler and can avoid auxiliary consumptions. The MEA design also differs in both, convective and passive cells, to take into account the different transport regimes. Whereas a more hydrophobic cathode will be preferred for the convective operation for the reasons explained in the previous section (Figures 11, 12), the passive

operation benefits from having larger hydrophobicity in the anode to avoid excess humidification and passing of liquid water to the anodic chamber coming from the air-breathing cathode. Passive cell operation is of higher technological interest in small and portable applications (Neațu et al., 2021).

4 Summary and outlook

Lowering Pt loading in next-generation polymer electrolyte fuel cells (PEFCs) is a priority to reduce their cost and make them more competitive. However, achieving high performance and durability at low Pt loading is hindered by significant local oxygen transport resistance around catalyst sites. The major contributors to local oxygen blockage are: i) oxygen adsorption at ionomer and Pt interfaces, and ii) oxygen diffusion across ionomer and water films, especially the former. The local oxygen transport resistance largely depends on operating conditions (relative humidity and temperature), ionomer content, morphology and uniformity, porosity of carbon support, and catalyst dispersity. Improving oxygen transport at low Pt loading demands an optimized design of the multiscale pore structure of the membrane electrode assembly (MEA), with a focus on the catalyst layer (CL). Operating conditions, materials cost, and components manufacture must be considered simultaneously.

At the smallest, nanometric scale, optimal accessibility of reaction sites to gas molecules and protons is the main objective. With this aim, appropriate starting materials (carbon support, ionomer), catalyst (Pt/C) synthesis method, and CL deposition methods may lead to the desired reduction in mass transport resistances. Appropriate disposition of the ionomer phase around the catalyst particles should be achieved to minimize transport resistances around the local reaction environment, especially at low catalyst loadings. Liquid water management must be adequate to provide protonic conductivity in the CL through a liquid path but avoiding pore flooding. With this aim, the use of deposition techniques for CL preparation, such as electro spraying, gives rise to a very convenient porous morphology with lower mass transport resistance.

Author contributions

PG-S: Conceptualization, Data curation, Formal Analysis, Funding acquisition, Investigation, Methodology, Project administration, Resources, Software, Supervision, Validation, Visualization, Writing—original draft, Writing—review and editing. PD: Conceptualization, Data curation, Formal Analysis, Investigation, Methodology, Resources, Validation, Visualization, Writing—original draft, Writing—review and editing. AC: Conceptualization, Data curation, Formal Analysis, Funding acquisition, Investigation, Methodology, Resources, Validation, Visualization, Writing—original draft, Writing—review and editing.

Funding

The author(s) declare that financial support was received for the research, authorship, and/or publication of this article. This work

was supported by projects PID2019-106740RBI00 and PORHYDRO1 TED2021-131620B-C21 of the Spanish Research Council, and by project PORHYDRO2 TED2021-131620B-C22/AEI European Union NextGenerationEU/PRTR, of the Ministry of Science and Innovation of Spain, Spanish Research Council.

Conflict of interest

The authors declare that the research was conducted in the absence of any commercial or financial relationships that could be construed as a potential conflict of interest.

References

- Avcioğlu, G. S., Fıccılar, B., Bayrakceken, A., and Eroğlu, I. (2015). High performance PEM fuel cell catalyst layers with hydrophobic channels. *Int. J. Hydrogen Energy* 40, 7720–7731. doi:10.1016/j.ijhydene.2015.02.004
- Baker, D. R., Caulk, D., Neyerlin, K. C., and Murphy, M. W. (2009). Measurement of oxygen transport resistance in PEM fuel cells by limiting current methods. *J. Electrochem. Soc.* 156, B991. doi:10.1149/1.3152226
- Benítez, R., Chaparro, A. M., and Daza, L. (2005). Electrochemical characterisation of Pt/C suspensions for the reduction of oxygen. *J. Power Sources* 151, 2–10. doi:10.1016/j.jpowsour.2005.02.077
- Berlinger, S. A., Garg, S., and Weber, A. Z. (2021). Multicomponent, multiphase interactions in fuel-cell inks. *Curr. Opin. Electrochem.* 29, 100744. doi:10.1016/j.coelec.2021.100744
- Borup, R. L., Kusoglu, A., Neyerlin, K. C., Mukundan, R., Ahluwalia, R. K., Cullen, D. A., et al. (2020). Recent developments in catalyst-related PEM fuel cell durability. *Curr. Opin. Electrochem.* 21, 192–200. doi:10.1016/j.coelec.2020.02.007
- Brodt, M., Han, T., Dale, N., Niangar, E., Wycisk, R., and Pintauro, P. (2015). Fabrication, *in-situ* performance, and durability of nanofiber fuel cell electrodes. *J. Electrochem. Soc.* 162, F84–F91. doi:10.1149/2.0651501jes
- Cetinbas, F. C., Advani, S. G., and Prasad, A. K. (2014). Investigation of a polymer electrolyte membrane fuel cell catalyst layer with bidirectionally-graded composition. *J. Power Sources* 270, 594–602. doi:10.1016/j.jpowsour.2014.07.148
- Cetinbas, F. C., Ahluwalia, R. K., Kariuki, N. N., De Andrade, V., and Myers, D. J. (2020). Effects of porous carbon morphology, agglomerate structure and relative humidity on local oxygen transport resistance. *J. Electrochem. Soc.* 167, 013508. doi:10.1149/2.0082001jes
- Chaparro, A. M., Ferreira-Aparicio, P., Folgado, M. A., Brightman, E., and Hinds, G. (2016). Study of superhydrophobic electrospayed catalyst layers using a localized reference electrode technique. *J. Power Sources* 325, 609–619. doi:10.1016/j.jpowsour.2016.06.077
- Chaparro, A. M., Ferreira-Aparicio, P., Folgado, M. A., Martín, A. J., and Daza, L. (2011). Catalyst layers for proton exchange membrane fuel cells prepared by electrospay deposition on Nafion membrane. *J. Power Sources* 196, 4200–4208. doi:10.1016/j.jpowsour.2010.09.096
- Chen, G. Y., Wang, C., Lei, Y. J., Zhang, J., Mao, Z., Mao, Z. Q., et al. (2017). Gradient design of Pt/C ratio and Nafion content in cathode catalyst layer of PEMFCs. *Int. J. Hydrog. Energy* 42, 29960–29965. doi:10.1016/j.ijhydene.2017.06.229
- Chen, M., Zhao, C., Sun, F., Fan, J., Li, H., and Wang, H. (2020). Research progress of catalyst layer and interlayer interface structures in membrane electrode assembly (MEA) for proton exchange membrane fuel cell (PEMFC) system. *eTransportation* 5, 100075. doi:10.1016/j.etrans.2020.100075
- Cheng, X., Shen, S., Wei, G., Wang, C., Luo, L., and Zhang, J. (2022a). Perspectives on challenges and achievements in local oxygen transport of low Pt proton exchange membrane fuel cells. *Adv. Mat. Technol.* 7, 2200228. doi:10.1002/admt.202200228
- Cheng, X., Wei, G., Wang, C., Shen, S., and Zhang, J. (2021). Experimental probing of effects of carbon support on bulk and local oxygen transport resistance in ultra-low Pt PEMFCs. *Int. J. Heat. Mass Transf.* 164, 120549. doi:10.1016/j.ijheatmasstransfer.2020.120549
- Cheng, X., You, J., Shen, S., Wei, G., Yan, X., Wang, C., et al. (2022b). An ingenious design of nanoporous nafion film for enhancing the local oxygen transport in cathode catalyst layers of PEMFCs. *Chem. Eng. J.* 439, 135387. doi:10.1016/j.cej.2022.135387
- Cho, J. H., Kim, J. M., Prabhuram, J., Hwang, S. Y., Ahn, D. J., Ha, H. Y., et al. (2009). Fabrication and evaluation of membrane electrode assemblies by low-temperature decal methods for direct methanol fuel cells. *J. Power Sources* 187, 378–386. doi:10.1016/j.jpowsour.2008.10.111
- Cho, S., Tamoto, K., and Uchida, M. (2020). Effect of an electrospay-generated ionomer morphology on polymer electrolyte fuel cell performance. *Energy Fuels* 34, 14853–14863. doi:10.1021/acs.energyfuels.0c02337
- Choo, M. J., Oh, K. H., Park, J. K., and Kim, H. T. (2015). Analysis of oxygen transport in cathode catalyst layer of low-Pt-loaded fuel cells. *ChemElectroChem* 2, 382–388. doi:10.1002/celc.201402354
- Conde, J., Ferreira-Aparicio, P., and Chaparro, A. (2021). Electrospay deposition: a breakthrough technique for proton exchange membrane fuel cell catalyst layer fabrication. *ACS Appl. Energy Mat.* 4, 7394–7404. doi:10.1021/acsaem.1c01445
- Conde, J. J., Folgado, M. A., Ferreira-Aparicio, P., Chaparro, A. M., Chowdhury, A., Kusoglu, A., et al. (2019). Mass-transport properties of electrospayed Pt/C catalyst layers for polymer-electrolyte fuel cells. *J. Power Sources* 427, 250–259. doi:10.1016/j.jpowsour.2019.04.079
- Cullen, D. A., Neyerlin, K. C., Ahluwalia, R. K., Mukundan, R., More, K. L., Borup, R. L., et al. (2021). New roads and challenges for fuel cells in heavy-duty transportation. *Nat. Energy* 6, 462–474. doi:10.1038/s41560-021-00775-z
- Darling, R. M., and Burlatsky, S. F. (2020). Modeling oxygen transport in high surface area carbon supports for polymer-electrolyte fuel cells. *J. Electrochem. Soc.* 167, 104506. doi:10.1149/1945-7111/ab9722
- Daş, E., Alkan Gürsel, S., Işikel Şanlı, L., and Bayrakceken Yurtcan, A. (2017). Thermodynamically controlled Pt deposition over graphene nanoplatelets: effect of Pt loading on PEM fuel cell performance. *Int. J. Hydrogen Energy* 42, 19246–19256. doi:10.1016/j.ijhydene.2017.06.108
- Das, P. K., Barbir, F., Jiao, K., Wang, Y., and Li, X. (2023). "Chapter 1 - fuel cells for transportation—an overview," in *Fuel cells for transportation*. Editors P. K. Das, K. Jiao, Y. Wang, B. Frano, and X. Li (Sawston, UK: Woodhead Publishing), 1–28.
- Das, P. K., Li, X., and Liu, Z. S. (2010). Analysis of liquid water transport in cathode catalyst layer of PEM fuel cells. *Int. J. Hydrogen Energy* 35, 2403–2416. doi:10.1016/j.ijhydene.2009.12.160
- Fan, L., Tu, Z., and Chan, S. H. (2021). Recent development of hydrogen and fuel cell technologies: a review. *Energy Rep.* 7, 8421–8446. doi:10.1016/j.egy.2021.08.003
- Folgado, M. A., Conde, J. J., Ferreira-Aparicio, P., and Chaparro, A. M. (2018). Single cell study of water transport in PEMFCs with electrospayed catalyst layers. *Fuel Cells* 18, 602–612. doi:10.1002/fuce.201700217
- Ganesan, A., and Narayanasamy, M. (2019). Ultra-low loading of platinum in proton exchange membrane-based fuel cells: a brief review. *Renew. Sustain. Energy* 8, 18. doi:10.1007/s40243-019-0156-x
- García-Salaberri, P. A. (2023a). Proton exchange membranes for polymer electrolyte fuel cells: an analysis of perfluorosulfonic acid and aromatic hydrocarbon ionomers. *Sustain. Mat. Technol.* 38, e00727. doi:10.1016/j.susmat.2023.e00727
- García-Salaberri, P. A. (2023b). A numerical assessment of mitigation strategies to reduce local oxygen and proton transport resistances in polymer electrolyte fuel cells. *Materials* 16, 6935. doi:10.3390/ma16216935
- Garsany, Y., Atkinson, R. W., Sassini, M. B., Hjelm, R. M. E., Gould, B. D., and Swider-Lyons, K. E. (2018). Improving PEMFC performance using short-side-chain low-equivalent-weight PFSA ionomer in the cathode catalyst layer. *J. Electrochem. Soc.* 165, F381–F391. doi:10.1149/2.1361805jes
- Gostick, J. T. (2013). Random pore network modeling of fibrous PEMFC gas diffusion media using voronoi and delaunay tessellations. *J. Electrochem. Soc.* 160, F731–F743. doi:10.1149/2.009308jes
- Greszler, T. A., Caulk, D., and Sinha, P. (2012). The impact of platinum loading on oxygen transport resistance. *J. Electrochem. Soc.* 159, F831–F840. doi:10.1149/2.061212jes

- Grigoriev, S. A., Fateev, V. N., Pushkarev, A. S., Pushkareva, I. V., Ivanova, N. A., Kalinichenko, V. N., et al. (2018). Reduced graphene oxide and its modifications as catalyst supports and catalyst layer modifiers for PEMFC. *Materials* 11, 1405. doi:10.3390/ma11081405
- Guo, Y., Pan, F., Chen, W., Ding, Z., Yang, D., Li, B., et al. (2021). *The controllable design of catalyst inks to enhance pemfc performance: a review*. Springer: Singapore.
- Harzer, G. S., Orfanidi, A., El-Sayed, H., Madkikar, P., and Gasteiger, H. A. (2018). Tailoring catalyst morphology towards high performance for low Pt loaded PEMFC cathodes. *J. Electrochem. Soc.* 165, F770–F779. doi:10.1149/2.0311810jes
- Higuera, F. J. (2018). Structure of deposits formed from electrosprayed aggregates of nanoparticles. *J. Aerosol Sci.* 118, 45–58. doi:10.1016/j.jaerosci.2018.01.007
- Iden, H., Mashio, T., and Ohma, A. (2013b). Gas transport inside and outside carbon supports of catalyst layers for PEM fuel cells. *J. Electroanal. Chem.* 708, 87–94. doi:10.1016/j.jelechem.2013.09.011
- Iden, H., Takaichi, S., Furuya, Y., Mashio, T., Ono, Y., and Ohma, A. (2013a). Relationship between gas transport resistance in the catalyst layer and effective surface area of the catalyst. *J. Electroanal. Chem.* 694, 37–44. doi:10.1016/j.jelechem.2013.02.008
- Iranzo, A., Boillat, P., Salva, A., and Biesdorf, J. (2016). PEM fuel cell operation under air and O₂ feed: analysis of cell performance and liquid water distributions. *Fuel Cells* 16, 463–468. doi:10.1002/fuce.201500145
- Işikel Şanlı, L., Bayram, V., Ghobadi, S., Düzen, N., and Alkan Gürsel, S. (2017). Engineered catalyst layer design with graphene-carbon black hybrid supports for enhanced platinum utilization in PEM fuel cell. *Int. J. Hydrogen Energy* 42, 1085–1092. doi:10.1016/j.ijhydene.2016.08.210
- James, B. D., Huya-Kouadio, J. M., and Houchins, C. (2021). *Final report: mass production cost estimation of direct H₂ PEM fuel cell systems for transportation applications 2020*. Arlington, VA, USA: Strategic Analysis Inc.
- Jao, T. C., Jung, G. B., Shen, H. L., Yeh, C. C., and Su, Y. J. (2013). Ultrasonic spray coating for proton exchange membrane fuel cell. *Open J. Acoust.* 03, 33–37. doi:10.4236/oja.2013.33a006
- Jha, N., Ramesh, P., Bekyarova, E., Tian, X., Wang, F., Itkis, M. E., et al. (2013). Functionalized single-walled carbon nanotube-based fuel cell benchmarked against US DOE 2017 technical targets. *Sci. Rep.* 3, 2257–7. doi:10.1038/srep02257
- Jiao, K., Xuan, J., Du, Q., Bao, Z., Xie, B., Wang, B., et al. (2021). Designing the next generation of proton-exchange membrane fuel cells. *Nature* 595, 361–369. doi:10.1038/s41586-021-03482-7
- Jinnouchi, R., Kudo, K., Kitano, N., and Morimoto, Y. (2016). Molecular dynamics simulations on O₂ permeation through nafion ionomer on platinum surface. *Electrochim. Acta* 188, 767–776. doi:10.1016/j.electacta.2015.12.031
- Kai, Y., Kitayama, Y., Omiya, M., Uchiyama, T., and Kumei, H. (2014). *In situ* observation of deformation behavior of membrane electrode assembly under humidity cycles. *J. Fuel Cell Sci. Technol.* 11, 051006. doi:10.1115/1.4028155
- Kannan, A. M., Veedu, V. P., Munukutla, L., and Ghasemi-Nejhad, M. N. (2007). Nanostructured gas diffusion and catalyst layers for proton exchange membrane fuel cells. *Electrochem. Solid-State Lett.* 10, 47–50. doi:10.1149/1.2422751
- Khodabakhshi, S., Fulvio, P. F., and Andreoli, E. (2020). Carbon black reborn: structure and chemistry for renewable energy harnessing. *Carbon N. Y.* 162, 604–649. doi:10.1016/j.carbon.2020.02.058
- Kim, Y., Lee, D., Kwon, Y., Kim, T. W., Kim, K., and Kim, H. J. (2019). Enhanced electrochemical oxygen reduction reaction performance with Pt nanocluster catalysts supported on microporous graphene-like 3D carbon. *J. Electroanal. Chem.* 838, 89–93. doi:10.1016/j.jelechem.2019.02.035
- Kongkanand, A., and Mathias, M. F. (2016). The priority and challenge of high-power performance of low-platinum proton-exchange membrane fuel cells. *J. Phys. Chem. Lett.* 7, 1127–1137. doi:10.1021/acs.jpclett.6b00216
- Kudo, K., Jinnouchi, R., and Morimoto, Y. (2016). Humidity and temperature dependences of oxygen transport resistance of nafion thin film on platinum electrode. *Electrochim. Acta* 209, 682–690. doi:10.1016/j.electacta.2016.04.023
- Kurihara, Y., Mabuchi, T., and Tokumasu, T. (2017). Molecular analysis of structural effect of ionomer on oxygen permeation properties in PEFC. *J. Electrochem. Soc.* 164, F628–F637. doi:10.1149/2.1301706jes
- Kurihara, Y., Mabuchi, T., and Tokumasu, T. (2019). Molecular dynamics study of oxygen transport resistance through ionomer thin film on Pt surface. *J. Power Sources* 414, 263–271. doi:10.1016/j.jpowsour.2019.01.011
- Kusoglu, A., and Weber, A. Z. (2017). New insights into perfluorinated sulfonic-acid ionomers. *Chem. Rev.* 117, 987–1104. doi:10.1021/acs.chemrev.6b00159
- Li, H., Tang, Y., Wang, Z., Shi, Z., Wu, S., Song, D., et al. (2008). A review of water flooding issues in the proton exchange membrane fuel cell. *J. Power Sources* 178, 103–117. doi:10.1016/j.jpowsour.2007.12.068
- Litster, S., and McLean, G. (2004). PEM fuel cell electrodes. *J. Power Sources* 130, 61–76. doi:10.1016/j.jpowsour.2003.12.055
- Liu, H., Epting, W. K., and Litster, S. (2015). Gas transport resistance in polymer electrolyte thin films on oxygen reduction reaction catalysts. *Langmuir* 31, 9853–9858. doi:10.1021/acs.langmuir.5b02487
- Liu, P., Yang, D., Li, B., Zhang, C., and Ming, P. (2023b). Recent progress of catalyst ink for roll-to-roll manufacturing paired with slot die coating for proton exchange membrane fuel cells. *Int. J. Hydrogen Energy* 48, 19666–19685. doi:10.1016/j.ijhydene.2023.02.022
- Liu, S., Yuan, S., Liang, Y., Li, H., Xu, Z., Xu, Q., et al. (2023a). Engineering the catalyst layers towards enhanced local oxygen transport of Low-Pt proton exchange membrane fuel cells: materials, designs, and methods. *Int. J. Hydrogen Energy* 48, 4389–4417. doi:10.1016/j.ijhydene.2022.10.249
- Liu, Y., Ji, C., Gu, W., Jorne, J., and Gasteiger, H. A. (2011a). Effects of catalyst carbon support on proton conduction and cathode performance in PEM fuel cells. *J. Electrochem. Soc.* 158, B614–B621. doi:10.1149/1.3562945
- Liu, Y., Ji, C., Gu, W., Jorne, J., and Gasteiger, H. A. (2011b). Effects of catalyst carbon support on proton conduction and cathode performance in PEM fuel cells. *J. Electrochem. Soc.* 158, B614–B621. doi:10.1149/1.3562945
- Lübben, L., Kirsch, S., Kadyk, T., and Eikerling, M. (2023). Test procedure for the prediction of water transport in polymer electrolyte fuel cells. *J. Power Sources* 556, 232504. doi:10.1016/j.jpowsour.2022.232504
- Macaulley, N., Lousenberg, R. D., Spinetta, M., Zhong, S., Yang, F., Judge, W., et al. (2022). Highly durable fluorinated high oxygen permeability ionomers for proton exchange membrane fuel cells. *Adv. Energy Mat.* 12, 2201063. doi:10.1002/aenm.202201063
- Malekian, A., Salari, S., Stumper, J., Djilali, N., and Bahrami, M. (2019). Effect of compression on pore size distribution and porosity of PEM fuel cell catalyst layers. *Int. J. Hydrog. Energy* 44, 23396–23405. doi:10.1016/j.ijhydene.2019.07.036
- Martin, S., García-Ybarra, P. L., and Castillo, J. L. (2010). High platinum utilization in ultra-low Pt loaded PEM fuel cell cathodes prepared by electrospraying. *Int. J. Hydrogen Energy* 35, 10446–10451. doi:10.1016/j.ijhydene.2010.07.069
- McNeary, W. W., Linico, A. E., and Weimer, A. W. (2020). Water management implications for ALD-modified polymer electrolyte membrane fuel cell catalysts. *J. Nanoparticle Res.* 22, 185. doi:10.1007/s11051-020-04921-8
- Mohseninia, A., Kartouzian, D., Eppler, M., Langner, P., Markötter, H., Wilhelm, F., et al. (2020). Influence of structural modification of micro-porous layer and catalyst layer on performance and water management of PEM fuel cells: hydrophobicity and porosity. *Fuel Cells* 20, 469–476. doi:10.1002/fuce.201900203
- Mulone, V., and Karan, K. (2013). Analysis of capillary flow driven model for water transport in PEFC cathode catalyst layer: consideration of mixed wettability and pore size distribution. *Int. J. Hydrogen Energy* 38, 558–569. doi:10.1016/j.ijhydene.2012.07.107
- Murata, S., Imanishi, M., Hasegawa, S., and Namba, R. (2014). Vertically aligned carbon nanotube electrodes for high current density operating proton exchange membrane fuel cells. *J. Power Sources* 253, 104–113. doi:10.1016/j.jpowsour.2013.11.073
- Nagamori, K., Aoki, S., Ikegawa, M., Tamoto, K., Honda, Y., Seki, Y., et al. (2023). Impacts of Pt/carbon black catalyst surface hydrophilicity on ionomer distribution and durability during water-generating load cycling of polymer electrolyte fuel cells. *ACS Appl. Energy Mat.* 6, 11481–11496. doi:10.1021/acsaem.3c01706
- Neatu, Ş., Neatu, F., Chirica, I. M., Borbáth, I., Tálas, E., Tompos, A., et al. (2021). Recent progress in electrocatalysts and electrodes for portable fuel cells. *J. Mat. Chem. A* 9, 17065–17128. doi:10.1039/d1ta03644k
- Nguyen, H., Sultanova, D., Heizmann, P. A., Vierrath, S., and Breitwieser, M. (2022). Improving the efficiency of fully hydrocarbon-based proton-exchange membrane fuel cells by ionomer content gradients in cathode catalyst layers. *Mat. Adv.* 3, 8460–8468. doi:10.1039/d2ma00761d
- Nonoyama, N., Okazaki, S., Weber, A. Z., Ikogi, Y., and Yoshida, T. (2011). Analysis of oxygen-transport diffusion resistance in proton-exchange-membrane fuel cells. *J. Electrochem. Soc.* 158, B416. doi:10.1149/1.3546038
- Ono, Y., Mashio, T., Takaichi, S., Ohma, A., Kanesaka, H., and Shinohara, K. (2010). The analysis of performance loss with low platinum loaded cathode catalyst layers. *ECs Trans.* 28, 69–78. doi:10.1149/1.3496614
- Ono, Y., Ohma, A., Shinohara, K., and Fushinobu, K. (2013). Influence of equivalent weight of ionomer on local oxygen transport resistance in cathode catalyst layers. *J. Electrochem. Soc.* 160, F779–F787. doi:10.1149/2.040308jes
- Orfanidi, A., Madkikar, P., El-Sayed, H. A., Harzer, G. S., Kratky, T., and Gasteiger, H. A. (2017). The key to high performance low Pt loaded electrodes. *J. Electrochem. Soc.* 164, F418–F426. doi:10.1149/2.1621704jes
- Ott, S., Orfanidi, A., Schmies, H., Anke, B., Nong, H. N., Hübner, J., et al. (2020). Ionomer distribution control in porous carbon-supported catalyst layers for high-power and low Pt-loaded proton exchange membrane fuel cells. *Nat. Mat.* 19, 77–85. doi:10.1038/s41563-019-0487-0
- Owejan, J. P., Owejan, J. E., and Gu, W. (2013). Impact of platinum loading and catalyst layer structure on PEMFC performance. *J. Electrochem. Soc.* 160, F824–F833. doi:10.1149/2.072308jes
- Padgett, E., Andrejevic, N., Liu, Z., Kongkanand, A., Gu, W., Moriyama, K., et al. (2018). Editors' choice—connecting fuel cell catalyst nanostructure and accessibility using quantitative cryo-STEM tomography. *J. Electrochem. Soc.* 165, F173–F180. doi:10.1149/2.0541803jes

- Paul, M. T. Y., Kim, D., Saha, M. S., Stumper, J., and Gates, B. D. (2020). Patterning catalyst layers with microscale features by soft lithography techniques for proton exchange membrane fuel cells. *ACS Appl. Energy Mat.* 3, 478–486. doi:10.1021/acsaem.9b01754
- Pollet, B. G., Kocha, S. S., and Staffell, I. (2019). Current status of automotive fuel cells for sustainable transport. *Curr. Opin. Electrochem.* 16, 90–95. doi:10.1016/j.coelec.2019.04.021
- Poojary, S., Islam, M. N., Shrivastava, U. N., Roberts, E. P. L., and Karan, K. (2020). Transport and electrochemical interface properties of ionomers in low-Pt loading catalyst layers: effect of ionomer equivalent weight and relative humidity. *Molecules* 25, 3387. doi:10.3390/molecules25153387
- Ramaswamy, N., Gu, W., Ziegelbauer, J. M., and Kumaraguru, S. (2020). Carbon support microstructure impact on high current density transport resistances in PEMFC cathode. *J. Electrochem. Soc.* 167, 064515. doi:10.1149/1945-7111/ab819c
- Ramaswamy, N., Kumaraguru, S., Koestner, R., Fuller, T., Gu, W., Kariuki, N., et al. (2021). Editors' choice—ionomer side chain length and equivalent weight impact on high current density transport resistances in PEMFC cathodes. *J. Electrochem. Soc.* 168, 024518. doi:10.1149/1945-7111/abe5eb
- Roh, C. W., Choi, J., and Lee, H. (2018). Hydrophilic-hydrophobic dual catalyst layers for proton exchange membrane fuel cells under low humidity. *Electrochem. Commun.* 97, 105–109. doi:10.1016/j.elecom.2018.11.003
- Rolfi, A., Oldani, C., Merlo, L., Facchi, D., and Ruffo, R. (2018). New perfluorinated ionomer with improved oxygen permeability for application in cathode polymeric electrolyte membrane fuel cell. *J. Power Sources* 396, 95–101. doi:10.1016/j.jpowsour.2018.05.093
- Sabarirajan, D. C., Liu, J., Qi, Y., Perego, A., Haug, A. T., and Zenyuk, I. V. (2020). Determining proton transport in pseudo catalyst layers using hydrogen pump DC and AC techniques. *J. Electrochem. Soc.* 167, 084521. doi:10.1149/1945-7111/ab927d
- Sakai, K., Sato, K., Mashio, T., Ohma, A., Yamaguchi, K., and Shinohara, K. (2009). Analysis of reactant gas transport in catalyst layers; effect of Pt-loadings. *ECS Trans.* 25, 1193–1201. doi:10.1149/1.3210674
- Sánchez-Ramos, A., Gostick, J. T., and García-Salaberri, P. A. (2021). Modeling the effect of low Pt loading cathode catalyst layer in polymer electrolyte fuel cells: Part I. Model formulation and validation. *J. Electrochem. Soc.* 168, 124514. doi:10.1149/1945-7111/ac4456
- Sánchez-Ramos, A., Gostick, J. T., and García-Salaberri, P. A. (2022). Modeling the effect of low Pt loading cathode catalyst layer in polymer electrolyte fuel cells. Part II: parametric analysis. *J. Electrochem. Soc.* 169, 074503. doi:10.1149/1945-7111/ac811d
- Sassin, M. B., Garsany, Y., Gould, B. D., and Swider-Lyonsa, K. (2016). Impact of compressive stress on MEA pore structure and its consequence on PEMFC performance. *J. Electrochem. Soc.* 163, F808–F815. doi:10.1149/2.0291608jes
- Schuler, T., Chowdhury, A., Freiberg, A. T., Sneed, B., Spingler, F. B., Tucker, M. C., et al. (2019). Fuel-cell catalyst-layer resistance via hydrogen limiting-current measurements. *J. Electrochem. Soc.* 166, F3020–F3031. doi:10.1149/2.0031907jes
- Sharma, S., and Pollet, B. G. (2012). Support materials for PEMFC and DMFC electrocatalysts - a review. *J. Power. Sources* 208, 96–119. doi:10.1016/j.jpowsour.2012.02.011
- Shen, S., Cheng, X., Wang, C., Yan, X., Ke, C., Yin, J., et al. (2017). Exploration of significant influences of the operating conditions on the local O₂ transport in proton exchange membrane fuel cells (PEMFCs). *Phys. Chem. Chem. Phys.* 19, 26221–26229. doi:10.1039/c7cp04837h
- Shen, W., Li, Z., and Liu, Y. (2008). Surface chemical functional groups modification of porous carbon. *Recent Pat. Chem. Eng.* 1, 27–40. doi:10.2174/2211334710801010027
- Shukla, S., Domican, K., Karan, K., Bhattacharjee, S., and Secanell, M. (2014). Analysis of low platinum loading thin polymer electrolyte fuel cell electrodes prepared by inkjet printing. *Electrochim. Acta* 156, 289–300. doi:10.1016/j.electacta.2015.01.028
- Sun, F., Liu, H., Chen, M., and Wang, H. (2023). Boosting oxygen transport through mitigating the interaction between Pt and ionomer in proton exchange membrane fuel cell. *J. Power Sources* 553, 232240. doi:10.1016/j.jpowsour.2022.232240
- Sun, X., Yu, H., Gao, X., and Shao, Z. (2021). The threshold method in the analysis of catalyst layer porosity towards oxygen transport resistance in PEMFCs. *Catal. Sci. Technol.* 11, 6804–6810. doi:10.1039/d1cy00882j
- Sun, X., Yu, H., Zhou, L., Gao, X., Zeng, Y., Yao, D., et al. (2020). Influence of platinum dispersy on oxygen transport resistance and performance in PEMFC. *Electrochim. Acta* 332, 135474. doi:10.1016/j.electacta.2019.135474
- Takahashi, K., Kakinuma, K., and Uchida, M. (2016). Improvement of cell performance in low-Pt-loading PEFC cathode catalyst layers prepared by the electrospray method. *J. Electrochem. Soc.* 163, F1182–F1188. doi:10.1149/2.0611610jes
- Tempelaere, M., Zimmermann, M., and Chatenet, M. (2023). 3D-structured electrocatalysts for improved mass-transfer in proton-exchange membrane fuel cell cathodes. *Curr. Opin. Electrochem.* 41, 101353. doi:10.1016/j.coelec.2023.101353
- Turtayeva, Z., Xu, F., Dillet, J., Mozet, K., Peignier, R., Celzard, A., et al. (2022). Manufacturing catalyst-coated membranes by ultrasonic spray deposition for PEMFC: identification of key parameters and their impact on PEMFC performance. *Int. J. Hydrogen Energy* 47, 16165–16178. doi:10.1016/j.ijhydene.2022.03.043
- Uchida, M. (2020). PEFC catalyst layers: effect of support microstructure on both distributions of Pt and ionomer and cell performance and durability. *Curr. Opin. Electrochem.* 21, 209–218. doi:10.1016/j.coelec.2020.02.019
- Uchida, M., Aoyama, Y., Eda, N., and Ohta, A. (1995a). Investigation of the microstructure in the catalyst layer and effects of both perfluorosulfonate ionomer and PTFE-loaded carbon on the catalyst layer of polymer electrolyte fuel cells. *J. Electrochem. Soc.* 142, 4143–4149. doi:10.1149/1.2048477
- Uchida, M., Aoyama, Y., Eda, N., and Ohta, A. (1995b). New preparation method for polymer-electrolyte fuel cells. *J. Electrochem. Soc.* 142, 463–468. doi:10.1149/1.2044068
- Uchida, M., Fukuoka, Y., Sugawara, Y., Eda, N., and Ohta, A. (1996). Effects of microstructure of carbon support in the catalyst layer on the performance of polymer-electrolyte fuel cells. *J. Electrochem. Soc.* 143, 2245–2252. doi:10.1149/1.1836988
- U.S. Department of Energy, (2022). USA: U.S. Department of Energy. https://www.hydrogen.energy.gov/program_records.html. DOE hydrogen and fuel cells program record
- Vairavapandian, D., Vichchulada, P., and Lay, M. D. (2008). Preparation and modification of carbon nanotubes: review of recent advances and applications in catalysis and sensing. *Anal. Chim. Acta* 626, 119–129. doi:10.1016/j.aca.2008.07.052
- Wang, C., Cheng, X., Lu, J., Shen, S., Yan, X., Yin, J., et al. (2017). The experimental measurement of local and bulk oxygen transport resistances in the catalyst layer of proton exchange membrane fuel cells. *J. Phys. Chem. Lett.* 8, 5848–5852. doi:10.1021/acs.jpclett.7b02580
- Wang, C., Cheng, X., Yan, X., Shen, S., Ke, C., Wei, G., et al. (2019). Respective influence of ionomer content on local and bulk oxygen transport resistance in the catalyst layer of PEMFCs with low Pt loading. *J. Electrochem. Soc.* 166, F239–F245. doi:10.1149/2.0401904jes
- Weber, A. Z., Balasubramanian, S., and Das, P. K. (2012). Chapter 2 - proton exchange membrane fuel cells. *Adv. Chem. Eng.* 41, 65–144. doi:10.1016/B978-0-12-386874-9.00003-8
- Weber, A. Z., and Kusoglu, A. (2014). Unexplained transport resistances for low-loaded fuel-cell catalyst layers. *J. Mat. Chem. A* 2, 17207–17211. doi:10.1039/c4ta02952f
- Wee, J. H. (2007). Applications of proton exchange membrane fuel cell systems. *Renew. Sustain. energy Rev.* 11, 1720–1738. doi:10.1016/j.rser.2006.01.005
- Whiston, M. M., Azevedo, I. L., Litster, S., Whitefoot, K. S., Samaras, C., and Whitacre, J. F. (2019). Expert assessments of the cost and expected future performance of proton exchange membrane fuel cells for vehicles. *Proc. Natl. Acad. Sci.* 116, 4899–4904. doi:10.1073/pnas.1804221116
- Woo, S., Lee, S., Taning, A. Z., Yang, T. H., Park, S. H., and Yim, S. D. (2020). Current understanding of catalyst/ionomer interfacial structure and phenomena affecting the oxygen reduction reaction in cathode catalyst layers of proton exchange membrane fuel cells. *Curr. Opin. Electrochem.* 21, 289–296. doi:10.1016/j.coelec.2020.03.006
- Yakovlev, Y. V., Lobko, Y. V., Vorokhta, M., Nováková, J., Mazur, M., Matolinová, I., et al. (2021). Ionomer content effect on charge and gas transport in the cathode catalyst layer of proton-exchange membrane fuel cells. *J. Power Sources* 490, 229531. doi:10.1016/j.jpowsour.2021.229531
- Yarlagadda, V., Carpenter, M. K., Moylan, T. E., Kukreja, R. S., Koestner, R., Gu, W., et al. (2018). Boosting fuel cell performance with accessible carbon mesopores. *ACS Energy Lett.* 3, 618–621. doi:10.1021/acsenergylett.8b00186
- Yarlagadda, V., Ramaswamy, N., Kukreja, R. S., and Kumaraguru, S. (2022). Ordered mesoporous carbon supported fuel cell cathode catalyst for improved oxygen transport. *J. Power Sources* 532, 231349. doi:10.1016/j.jpowsour.2022.231349
- Yoshino, S., Shinohara, A., Kodama, K., and Morimoto, Y. (2020). Fabrication of catalyst layer with ionomer nanofiber scaffolding for polymer electrolyte fuel cells. *J. Power Sources* 476, 228584. doi:10.1016/j.jpowsour.2020.228584
- Yue, M., Jemei, S., Zerhouni, N., and Gouriveau, R. (2021). Proton exchange membrane fuel cell system prognostics and decision-making: current status and perspectives. *Renew. Energy* 179, 2277–2294. doi:10.1016/j.renene.2021.08.045
- Zapardiel, D., and García-Salaberri, P. A. (2022). Modeling the interplay between water capillary transport and species diffusion in gas diffusion layers of proton exchange fuel cells using a hybrid computational fluid dynamics formulation. *J. Power Sources* 520, 230735. doi:10.1016/j.jpowsour.2021.230735
- Zhang, Q., Dong, S., Shao, P., Zhu, Y., Mu, Z., Sheng, D., et al. (2022). Covalent organic framework-based porous ionomers for high-performance fuel cells. *Science* 378, 181–186. doi:10.1126/science.abm6304
- Zhu, J., Holmen, A., and Chen, D. (2013). Carbon nanomaterials in catalysis: proton affinity, chemical and electronic properties, and their catalytic consequences. *ChemCatChem* 5, 378–401. doi:10.1002/cctc.201200471